Faculty of Physics and Astronomy

University of Heidelberg

Diploma thesis

in Physics

submitted by

Verena Fiedler

born in Freiburg

September 2004

The Atmospheric Aerosol Precursor Gas Sulphuric Acid: Mass Spectrometric Measurements in the Atmospheric Boundary Layer in Finland and Germany.

This diploma thesis has been carried out by Verena Fiedler at the
Max-Planck-Institute for Nuclear Physics, Heidelberg
(Atmospheric physics division)
under supervision of
Prof. Dr. Frank Arnold

The Atmospheric Aerosol Precursor Gas Sulphuric Acid: Mass Spectrometric Measurements in the Atmospheric Boundary Layer in Finland and Germany.

Measurements of gaseous sulphuric acid and aerosol particle data have been carried out in the atmospheric boundary layer in a relatively unpolluted region (Hyytiälä, Finland) and in a relatively polluted region (Heidelberg, Germany) by the MPI-K during the European project QUEST (Quantification of Aerosol Nucleation in the European Boundary Layer). Sulphuric acid has been measured via chemical ionization mass spectrometry (CIMS). The method, used in Heidelberg, and the measured sulphuric acid concentrations will be discussed in detail in this work. Aerosol particle data have been obtained using a differential mobility particle sizer (DMPS). From the measurements various quantities like growth, nucleation and condensable vapor source rates have been calculated. Moreover, the percentage contribution of sulphuric acid to particle formation and growth has been determined and the correlation of sulphuric acid to small particle formation has been investigated. Finally the influence of air mass trajectories has been examined.

Das atmosphärische Aerosol-Vorläufer-Gas Schwefelsäure: Massenspektrometrische Messungen in der atmosphärischen Grenzschicht in Finnland und Deutschland.

Messungen von gasförmiger Schwefelsäure und Aerosolpartikeln wurden im Rahmen des europäischen Projektes QUEST (Quantification of Aerosol Nucleation in the European Boundary Layer) in der atmosphärischen Grenzschicht einmal in relativ sauberer Region (Hyytiälä, Finnland) und einmal in relativ verschmutzter Region (Heidelberg, Deutschland) durchgeführt. Dabei wurde Schwefelsäure mittels chemischer Ionisations-Massenspektrometrie (CIMS) gemessen. Die in Heidelberg angewandte Methode, sowie die dort gemessenen Schwefelsäurekonzentrationen werden in dieser Arbeit vorgestellt. Aerosol-Partikeldaten wurden mit einem Differential Mobility Particle Sizer (DMPS) gewonnen. Mit Hilfe der Messungen wurden verschiedene Werte wie Wachstums- und Nukleationsraten, sowie Quellstärken des kondensierbaren Gases berechnet. Desweiteren wurde der prozentuale Anteil der Schwefelsäure an Nukleation und Wachstum der Partikel bestimmt und die Korrelation zwischen neugebildeten Teilchen und Schwefelsäure untersucht. Zum Abschluss wurde noch der Einfluss von Luftmassentrajektorien bewertet.

Contents

Chapter 1

Introduction

Aerosol particles are an ubiquitous component of the Earth's atmosphere and influence our life in many different ways. In a global view they might contribute to climate change due to their major role in atmospheric chemistry and their ability to interact directly with the solar and infrared terrestrial radiation fields [Ramanathan et al., 2001, Harshvardhan et al., 2002, Garrett et al., 2002]. A third important matter is their influence on the formation of cloud condensation nuclei (CCN) [Menon and Saxena, 1998].

Also humans can be directly affected, as aerosols may cause harm through inhalation [Stieb et al., 2002, Wichmann and Peters, 2000, Kim, 2000]. In order to understand, predict and finally prevent those effects a detailed investigation of the sources and growth mechanisms of aerosol particles is needed.

In recent years, the atmospheric trace gas sulphuric acid has been found to be a main candidate in producing new particles and in contributing to their subsequent growth [Reiner and Arnold, 1993, Reiner and Arnold, 1994, Boy et al., 2004, Kulmala, 2003]. It can participate in binary, ternary and ion induced nucleation [Arnold, 1982, Korhonen et al., 1999, Yue and Chan, 1979]. Therefore it is important to measure sulphuric acid and aerosol relevant parameters at the same time to quantify the contribution of sulphuric acid to particle formation and growth.

Within the European project QUEST (Quantification of Aerosol Nucleation in the European Boundary Layer) measurements of sulphuric acid and aerosol particle data were carried out in three different European regions. The aim of this project is to qualify and quantify

nucleation events in maritime, clean continental and polluted continental air.

During the last two campaigns sulphuric acid was measured by our group using chemical ionization mass spectrometry (CIMS). This method will be discussed in detail in chapter 3. In chapter 2 the principles of H_2SO_4-chemistry and aerosol theory will be presented. In this chapter also the importance of sulphuric acid for particle nucleation and growth will become obvious. Chapter 4 will describe the European QUEST-project in some detail. In chapter 5 the experimental setup to measure sulphuric acid and our calibration system will be explained. Finally the following three chapters will present the measured H_2SO_4 data and they will deal with the analysis and comparison of these data at our two measurement sites Hyytiälä, Finland and Heidelberg, Germany. For this comparison various quantities like growth, nucleation and vapor source rates of aerosols have been calculated, the percentage contribution of sulphuric acid to new particle formation and growth has been determined and the influence of air trajectories has been examined.

Chapter 2

Atmospheric Sulphuric Acid

In this chapter the main sources and sinks of atmospheric sulphuric acid in the troposphere will be explained and a short summary of aerosol dynamics and sulphuric acid nucleation theory will be given.

2.1 Sulphuric Acid

Sulphuric acid is an important trace gas in the atmosphere. Due to its low saturation vapor pressure, it condenses very easily on existent particles and forces their growth. Moreover, sulphuric acid is considered to be the most important vapor concerning nucleation and new particle formation. On the one hand a higher number of particles in the atmosphere increases the earth´s albedo (i.e. the percentage of radiation that is directly reflected back from the earth). On the other hand it contributes to longwave heating, as infrared radiation is reflected back to the earth from the particles. This is the reason why investigations and measurements of sulphuric acid are so important. Typical concentrations of H_2SO_4 in the atmosphere range from $1 \cdot 10^5$ to $1 \cdot 10^7 cm^{-3}$ which corresponds at a pressure of $1.013 \cdot 10^5$ Pa and a temperature of 293.15 K to 4 and 400 ppqv (parts per quadrillion by volume, 1 ppqv = 1 molecule H_2SO_4 in $1 \cdot 10^{15}$ atmospheric molecules).

2.1.1 Sources of gaseous H_2SO_4

The main reaction, that leads to the production of gaseous sulphuric acid in the troposphere is the following mechanism:

$$SO_2 + \cdot OH + M \longrightarrow HSO_3 \cdot + M,\ k_1 = 9 \cdot 10^{-13} cm^3 s^{-1} \tag{2.1}$$

$$HSO_3 \cdot + O_2 \longrightarrow SO_3 + HO_2 \cdot,\ k_2 = 4.3 \cdot 10^{-13} cm^3 s^{-1} \tag{2.2}$$

$$SO_3 + H_2O + M \longrightarrow H_2SO_4 + M. \tag{2.3}$$

In this reaction the temperature and pressure dependent step (2.1) is limiting (the indicated value for k is for a temperature of 295 K and a pressure of $1.0 \cdot 10^5$ Pa). The last step (2.3) is not completely understood yet. There are two possible pathways, how H_2SO_4 could be formed from SO_3 and water [Reiner and Arnold, 1993, Reiner and Arnold, 1994, Kolb et al., 1994, Lovejoy et al., 1996].

$$SO_3 + 2H_2O \longrightarrow H_2SO_4 + H_2O \tag{2.4}$$

$$SO_3(H_2O) + H_2O \longrightarrow H_2SO_4 + H_2O. \tag{2.5}$$

Although the rate constant of reaction (2.3) is not exactly known so far, it is definitely smaller than k_1 [Finlayson-Pitts and Pitts, 2000].

OH in the troposphere is mainly formed by the photolysis of ozone:

$$O_3 + h\nu \longrightarrow O(^1D) + O_2,\ (\lambda \leq 310\ nm) \tag{2.6}$$

$$O(^1D) + H_2O \longrightarrow 2 \cdot OH,\ k = 2.2 \cdot 10^{-10} cm^3 s^{-1} \tag{2.7}$$

$$O(^1D) + M \longrightarrow O(^3P) + M. \tag{2.8}$$

Ozone is photolyzed into oxygen and an excited O in singlet D state. 90 % of these excited oxygen atoms loose their energy through collisions with other molecules (M in step (2.8)) and usually recombine to oxygen [Finlayson-Pitts and Pitts, 2000]. About 10 % collide with water molecules which leads to OH formation according to reaction (2.7).

Other sources of OH are the photolysis of nitrous acid HONO and hydrogen peroxide H_2O_2. Due to its high reactivity, the OH-radical has only a lifetime of about 1 s under atmospheric conditions. Consequently, OH chemistry stops almost completely during nighttime.

Then another reaction could become an important source for H_2SO_4:

$$CH_3O_2 \cdot + SO_2 \longrightarrow CH_3O \cdot + SO_3 \tag{2.9}$$

SO_3 again forms sulphuric acid following reaction (2.3).

SO_2, which is necessary for reaction (2.1), has its origin in all kinds of combustion: Biomass burning, industry, traffic (these three factors are mainly responsible for tropospheric SO_2 release), in addition to that also natural sources like volcanoes are important (this SO_2 can be transported up to the stratosphere).

At this point it should just be mentioned that oxidants like H_2O_2 can also produce H_2SO_4 in the liquid phase by oxidizing SO_2 that is solved e.g. in a water droplet. This process is well known as acid deposition or, its more popular name, acid rain.
More details can be found in [Finlayson-Pitts and Pitts, 2000] and [Wayne, 2000].

2.1.2 Sinks of gaseous H_2SO_4

Self nucleation of H_2SO_4 requires very high concentrations of H_2SO_4 as well as low pre-existent water and particle concentrations. These conditions are usually not reached in the atmosphere. Consequently, the main removal mechanisms are condensation on solid aerosol particles or absorption in water droplets. In order to describe the mass transfer to a surface correctly aerosol dynamic theory is divided into three parts, using the so-called Knudsen-number as indicator. The Knudsen-number

$$Kn = \lambda / R_p \tag{2.10}$$

sets the mean free path λ of a molecule in a fluid in relation to a particle radius R_p:

- $Kn \ll 1$: Continuum regime. The particle "sees" the surrounding gas as a fluid. Fluid dynamics (Navier-Stokes etc.) can be applied in this case.
- $Kn \gg 1$: Free-molecular regime. Particles behave like free gas molecules. Kinetic gas theory comes to application here.
- $Kn \approx 1$: Transition regime. Dynamics are difficult to describe theoretically as it would be necessary to solve the Boltzmann-equation directly. Usually semi-empirical correlations are used in this case.

In principle one can say that for a particle whose radius is bigger than 200 nm continuum dynamics works and for a particle with a radius smaller than 10 nm kinetic gas theory can be applied.

The nowadays mostly used approximation for the transition regime is the approach by Fuchs and Sutugin [Fuchs and Sutugin, 1971]. In empirical studies they found a correction factor β_M that relates the mass flux J_{trans} of the transition regime to the mass flux J_{cont} of the continuum regime:

$$J_{trans} = \beta_M \cdot \ J_{cont} \tag{2.11}$$

with

$$\beta_M = \frac{\alpha \cdot (1 + Kn)}{\alpha \cdot (1 + 0.377Kn) + 1.33Kn + 1.33Kn^2} \tag{2.12}$$

α is the so-called mass accommodation coefficient i.e. the probability of a gas molecule to stick to the particle after collision (in some experiments this coefficient was found to be almost 1) [Weber et al., 1997]. With $\alpha = 1$ we get

$$J_{trans} = \frac{1 + Kn}{1 + 1.71Kn + 1.33Kn^2} \cdot \ J_{cont} \tag{2.13}$$

To get a loss rate L the mass fluxes of all particle sizes have to be summed up and multiplied with the particle number concentration:

$$L = \sum_i \frac{16\, N_i\, Kn_i\, \alpha\, v\, \pi\, R_{p_i}^2}{3\,\alpha + (3\,\alpha\, l_i + 4(1-\alpha))Kn_i} \tag{2.14}$$

with

$$l_i = \frac{0.71 + 1.333Kn_i}{1 + Kn_i} \tag{2.15}$$

N is the particle number concentration, R_p the particle diameter and v is the mean thermal velocity.

More about aerosol dynamics can be read in [Seinfeld and Pandis, 1998].

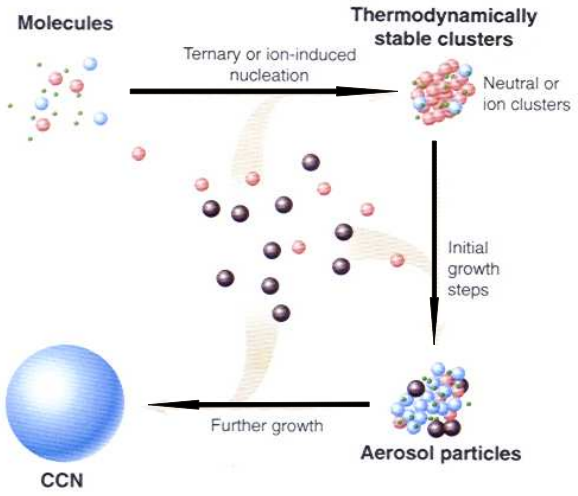

Figure 2.1: Scheme to illustrate the process of nucleation via binary, ternary or ion induced nucleation and further growth up to cloud condensation nuclei (CCN) [Kulmala, 2003].

2.2 Aerosol cycle

There are in principle two mechanisms how new particles are being formed in the atmosphere:

- Through homogeneous, heterogeneous or ion induced nucleation of originally gaseous compounds that coagulate and condensate onto preexistent particles.
- Through dispersion of dust or sea salt spray and water droplets.

The first point will be explained a bit further now as these are the mechanisms where sulphuric acid is involved in new particle formation. Again we need to distinguish between 4 different pathways:

- Homomolecular homogeneous nucleation: Only one type of molecules forms clusters through coagulation directly from the gas phase. This process requires such a high supersaturation of the condensable species, that it usually does not occur in free troposphere.
- Heteromolecular homogeneous nucleation: Two or more types of molecules form clusters through coagulation from the gas phase. The most important formation pathways found

so far are binary nucleation of H_2SO_4 and water and ternary nucleation of H_2SO_4, NH_3 and water.

- Heterogeneous nucleation: Condensation of one or more condensable species onto the surface of preexistent water droplets or particles.

- Ion induced nucleation: Accumulation of (charged or polarized) molecules on existent ions. This mechanism matters the most in the stratosphere and upper troposphere.

Figure 2.1 illustrates the formation of new particles via nucleation. Finally this leads to cloud condensation nuclei (CCN). At this point the relevance of nucleation concerning climate change patterns becomes clear as well. Formation of new CCN means more and specifically more small cloud droplets and therefore the lifetime of clouds is prolonged.

Nucleation theory is a very complex matter and can be presented here only fragmentarily. As an example the nucleation rate of classical binary nucleation theory will be derived very briefly. All other theories follow the same pattern, just starting from different Gibbs free energies.

Classical binary nucleation theory was first used by Flood, Volmer, Neumann, Döring and Reiss [Flood, 1934, Volmer, 1939, Neumann and Döring, 1940, Reiss, 1950]. They noted that a growing binary cluster can be thought of as moving on a saddle-shaped free energy surface, the saddle point corresponding to the critical cluster (critical cluster size means the size from which the cluster starts to be stable). The change of the Gibbs free energy of formation of a spherical binary liquid cluster from the vapor phase is [Reiss, 1950]:

$$\Delta G = n_1 \Delta\mu_1 + n_2 \Delta\mu_2 + 4\pi r^2 \sigma \tag{2.16}$$

with n_i being the number of the i'th species in the cluster, $\Delta\mu_i$ being the change of the chemical potential of species i between the vapor phase and the liquid phase, r being the radius of the cluster and σ the surface tension.

The total number n_i can be written as

$$n_i = n_i^s + n_i^b \tag{2.17}$$

where n_i^s indicates the number of surface molecules and n_i^b the number of interior ("bulk") molecules.

The saddle point on the free energy surface can be found setting

$$\left(\frac{\partial \Delta G}{\partial n_i}\right)_{n_j} = 0 \tag{2.18}$$

and this leads to the following two equations (by using the Gibbs-Duhem equation)

$$n_1^b d\mu_1^l + n_2^b d\mu_2^l = 0 \tag{2.19}$$

$$n_1^s d\mu_1^l + n_2^s d\mu_2^l + A d\sigma = 0 \tag{2.20}$$

and furthermore to the binary Kelvin equation:

$$\Delta\mu_i + \frac{2\sigma\nu_i}{r^*} = 0 \tag{2.21}$$

(ν_i are the partial molecular volumes: $n_1\nu_1 + n_2\nu_2 = \frac{4}{3}\pi r^3$).

So we find for the radius and the free energy of formation of the critical cluster:

$$r^* = -\frac{2\sigma\nu_i}{\Delta\mu_i} \tag{2.22}$$

$$\Delta G^* = \frac{4}{3}\pi r^{*2}\sigma \tag{2.23}$$

From there the nucleation rate J can be derived:

$$J = R_{ave} F Z \exp\left(-\Delta G^*/kT\right) \tag{2.24}$$

with R_{ave} being the average condensation rate, F is the number of molecular species in the vapor, Z is the Zeldovich non equilibrium factor (a numerical correction [Stauffer, 1976]), k is the Boltzmann constant and T the temperature.
In detail this derivation is far more complex, but a complete and detailed derivation can be found in [Seinfeld and Pandis, 1998].

The main removal mechanisms for aerosol particles in the atmosphere are dry and wet deposition. Particles, especially large ones, are settling down in the gravitational field of the earth (dry deposition) or are washed out ("scavenged") by rain (wet deposition). Both mechanisms lead to a change in the shape of the particle number distribution (smaller particles are

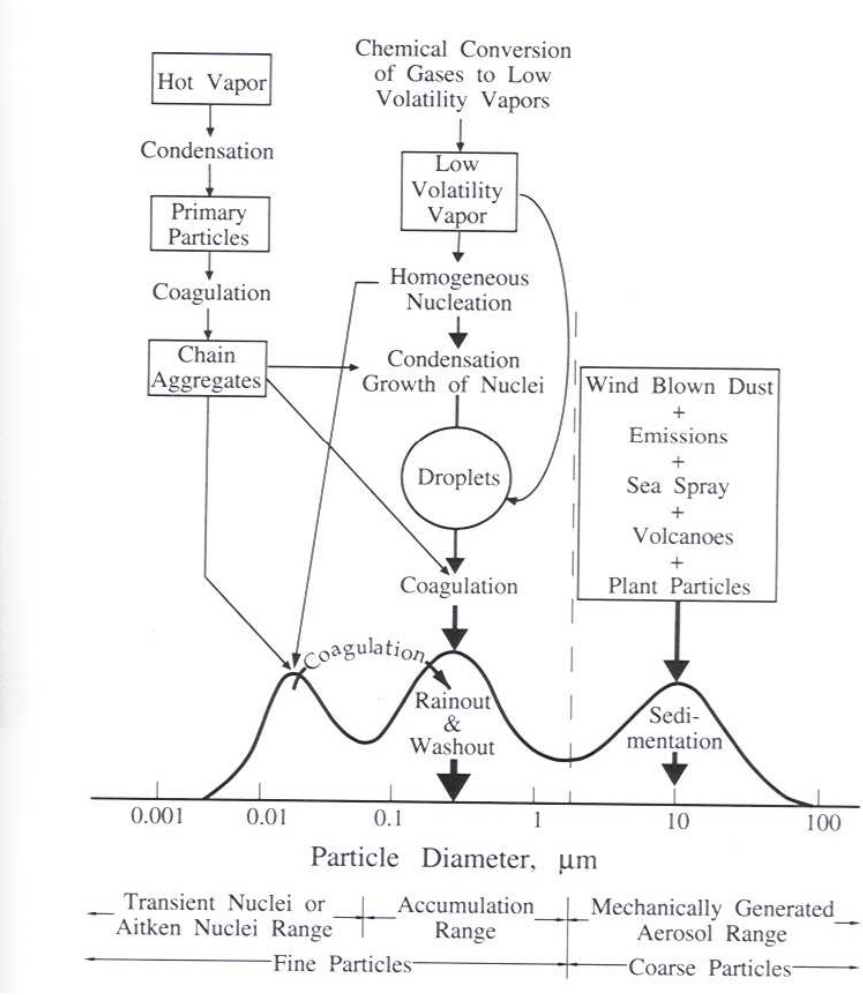

Figure 2.2: Overview of the main building and removal mechanisms of atmospheric aerosols [Seinfeld and Pandis, 1998].

"caught" by bigger ones, the distribution is shifted to higher particle diameters) and finally this reduces the total number of particles [Seinfeld and Pandis, 1998, Laakso et al., 2003].

Figure 2.2 summarizes the aerosol cycle and links the aggregation and removal mechanisms together. H_2SO_4 mainly contributes to the formation pathway in the middle (Chemical conversion of gases etc.).

Chapter 3

Sulphuric Acid Measurement Principle

Measurements of atmospheric trace gases like H_2SO_4 in the sub pptv range are a real challenge because of the very low concentration values (10^5 - 10^7 cm^{-3}, see chapter 2). During the QUEST campaign sulphuric acid was measured using chemical ionization mass spectrometry (CIMS), which bases on an ion molecule reaction (IMR) that was originally proposed by [Arnold, 1978, Arnold and Fabian, 1980, Arnold and Viggiano, 1980, Knop and Arnold, 1985] and further developed by [Eisele and Tanner, 1993]. The principle of this measurement method is to convert the hardly detectable trace gas into more easily detectable product ions through a highly efficient ion molecule reaction. Reactions of molecules with ions have a high cross section because of permanent or induced dipole moments. This is the reason for the high efficiency. Typical rate coefficients are around $10^{-9}cm^3s^{-1}$ compared to $10^{-11}cm^3s^{-1}$ in the case of a fast reaction between neutral molecules.

One needs to distinguish between active CIMS (ACIMS), in which the educt ions are produced artificially in an ion source, and passive CIMS (PACIMS), which employs the fact that also ions that naturally occur in the atmosphere can work as educt ions. The main elements of CIMS are a flow reactor, an ion source, a H_2SO_4-source used for calibration and a mass spectrometer for the ion detection (see **Figure 3.1**).

In this chapter, both the measurement principles and a short description of the theory of quadrupole storage mass spectrometry will be presented.

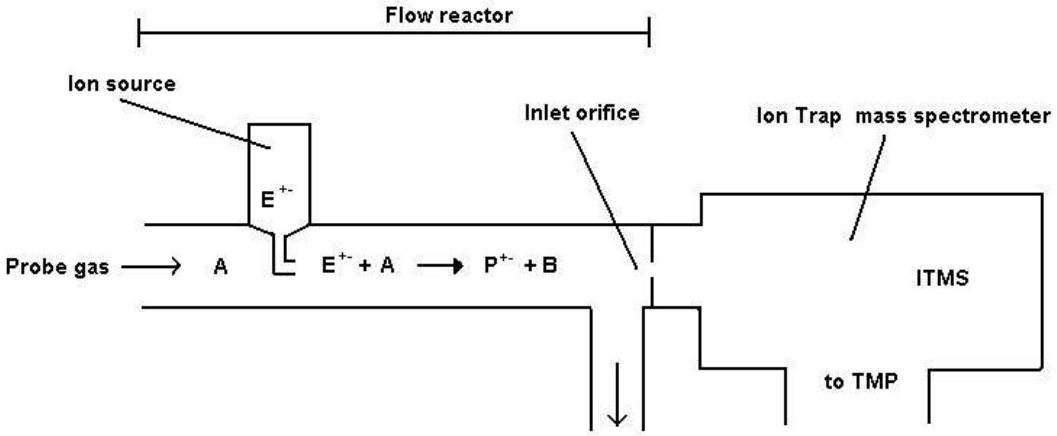

Figure 3.1: Principle scheme of a CIMS apparatus. (For the ITMS see Figure 3.5).

3.1 Ion-Molecule Reaction

Generally an IMR follows the reaction type

$$\mathrm{E}^{\pm} + \mathrm{A} \xrightarrow{k} \mathrm{P}^{\pm} + \mathrm{B} \tag{3.1}$$

where A are the neutral gas molecules that have to be measured, E are the educt ions, P the detectable product ions and B a neutral reaction product.

Moreover

$$\frac{d}{dt}[\mathrm{E}^{\pm}] = -\frac{d}{dt}[\mathrm{P}^{\pm}] = -k[\mathrm{E}^{\pm}][\mathrm{A}] \tag{3.2}$$

A can be assumed to be constant $[\mathrm{A}](t) = [\mathrm{A}]_0$, since there is a high surplus of A. Consequently equation (3.2) can be directly integrated to

$$[\mathrm{E}^{\pm}] = [\mathrm{E}^{\pm}]_0 \cdot e^{-k[\mathrm{A}]\mathrm{t}} \tag{3.3}$$

and as the charges are preserved ($[\mathrm{P}^{\pm}]+[\mathrm{E}^{\pm}]$=const.)

$$[\mathrm{P}^{\pm}] = [\mathrm{E}^{\pm}]_0 \cdot (1 - e^{-k[\mathrm{A}]t}) \tag{3.4}$$

Dividing equation (3.4) by equation (3.3) and solving for [A] we get the so-called **ACIMS-Formula**:

$$[\mathrm{A}] = \frac{1}{k \cdot t_{IMR}} \ln\left(1 + \frac{[\mathrm{P}^{\pm}]}{[\mathrm{E}^{\pm}]}\right) \tag{3.5}$$

The concentration of the neutral substance A can consequently be determined by measuring the product- and educt-ion-concentrations, if the rate constant k and the constant reaction time t_{IMR} is known.

Usually this reaction scheme becomes more complicated by the possibility that the educt ions can react with several different types of molecules:

$$\mathrm{E}^{\pm} + \mathrm{A}_i \longrightarrow \mathrm{P}_i^{\pm} + \mathrm{B_i} \tag{3.6}$$

Then the **Parallel-ACIMS-Formula** has to be used.

$$[\mathrm{A}_i] = \frac{1}{k \cdot t} \cdot \frac{[\mathrm{P}_i^{\pm}]}{\sum_{j=1}^{n}[\mathrm{P}_j^{\pm}]} \cdot \ln\left(1 + \frac{\sum_{j=1}^{n}[\mathrm{P}_j^{\pm}]}{[\mathrm{E}^{\pm}]}\right) \tag{3.7}$$

A detailed derivation of this formula can be found in [Wollny, 1998].

3.1.1 Measurements of sulphuric acid by CIMS

As an specific example the IMR used to measure sulphuric acid will be discussed in this section. The detection of gaseous sulphuric acid in the atmosphere is based on a reaction with $\mathrm{NO_3^-(HNO_3)}_n$ ions. The principle was proposed by [Arnold and Fabian, 1980] and further developed by [Arnold and Viggiano, 1980]. The reaction proceeds as follows:

$$\mathrm{NO_3^-(HNO_3)}_n + \mathrm{H_2SO_4} \xrightarrow{k_n} \mathrm{HSO_4^-(HNO_3)}_n + \mathrm{HNO_3} \tag{3.8}$$

The gas phase acidity of $\mathrm{HNO_3}$ is quite high, so that only a few substances like $\mathrm{H_2SO_4}$ with an even higher acidity will undergo reactions with $\mathrm{HNO_3}$-compounds. Therefore the $\mathrm{NO_3^-(HNO_3)}_n$ clusters are very stable with regard to proton transfer reactions and the upper IMR (3.8) is very selective [Arnold and Fabian, 1980, Viggiano et al., 1997]. Viggiano and coworkers also determined the rate coefficients k_n for reaction (3.8) in case of $n = 0, 1$ and 2 to 2.23, 1.86 and 1.72 $\cdot 10^{-9}$ cm^3 s^{-1} with an accuracy of about 10 to 15 %.

The ACIMS-formula (3.5) yields:

$$[\mathrm{H_2SO_4}] = \frac{1}{k \cdot t} \cdot \ln(1 + R) \tag{3.9}$$

with

$$R = \frac{\sum_n [\mathrm{HSO_4^-(HNO_3)}_n]}{\sum_n [\mathrm{NO_3^-(HNO_3)}_n]} \tag{3.10}$$

and k needs to be the weighted average of the k_n mentioned above.

It is obvious that for measurements of very low sulphuric acid concentrations either R has to be as small as possible, which corresponds to a high surplus of educt ions to product ions, or the reaction time t has to be as long as possible. The latter is however limited due to ion losses and reagent gas losses to the walls of the measurement device and due to ion-ion recombination, which concerns product ions as well as educt ions. The more losses and the lower absolute concentrations, the more electronic noise will become important. So, from an experimentalists point of view, it is important to figure out the best configuration of the devices to minimize losses of H_2SO_4 and to optimize the dynamic range of the instrument.

3.2 Quadrupole Storage Mass Spectrometry (QSMS)

The quadrupole mass filter was first proposed by W. Paul 1953 [Paul and Steinwedel, 1953, Paul and Raether, 1955, Paul et al., 1958]. The new invention was a mass spectrometer which used only electric fields for mass selection. Previously, mass spectrometers used magnetic fields which made the instruments usually big and unwieldy.

Later the instrument used during the Heidelberg-campaign, PITMAS (**P**aul **I**on **T**rap **Ma**ss **S**pectrometer) or IT-CIMS (**I**on **T**rap **C**hemical **I**onization **M**ass **S**pectrometer), will be described as an example for a very advanced QSMS technique. Yet first a short summary of the theory of quadrupole storage mass spectrometry will be given.

3.2.1 Theory

When a single ion experiences a quadrupole field, there is no space charge due to the presence of other charged particles and the field is then said to be ideal. In this case the potential ϕ at any point (x, y, z) within the field is called harmonic and may be expressed by the relationship

$$\phi = \frac{\phi_0}{r_0^2}(\lambda x^2 + \sigma y^2 + \gamma z^2) \tag{3.11}$$

where ϕ_0 is the applied electric potential, λ, σ and γ are weighting constants for the x, y and z coordinates and r_0 is a device dependent constant.

The applied potential is a combination of a radio frequency potential $V \cos \omega t$ and a direct current potential U:

$$\phi_0 = U - V \cos \omega t \tag{3.12}$$

with $\omega = 2\pi f$ (f the frequency of the field in Hz).

Equation (3.11) must satisfy Laplace´s equation:

$$\Delta \phi = 0 \tag{3.13}$$

This leads to the following condition, that has to be satisfied in all kind of quadrupole devices:

$$\lambda + \sigma + \gamma = 0 \tag{3.14}$$

or in trivial case $\phi_0 = 0$.

The force in x-direction experienced by an ion of mass m and charge e and likewise the forces in y- and z-direction may be expressed as

$$F_x = ma = m\frac{d^2x}{dt^2} = -e\frac{\partial \phi}{\partial x} \tag{3.15}$$

where a is the acceleration of the ion.

Substituting equation (3.12) for ϕ_0 in equation (3.11) and differentiating with respect to x, y and z yields the potential gradients. Furthermore this leads to the equations of motion of a single charged positive ion in an electric quadrupole field.

$$\frac{d^2x}{dt^2} + \frac{2\lambda e}{mr_0^2}(U - V \cos \omega t)x = 0 \tag{3.16}$$

$$\frac{d^2y}{dt^2} + \frac{2\sigma e}{mr_0^2}(U - V \cos \omega t)y = 0 \tag{3.17}$$

$$\frac{d^2z}{dt^2} + \frac{2\gamma e}{mr_0^2}(U - V \cos \omega t)z = 0. \tag{3.18}$$

By introducing the dimensionless parameter $\xi = \omega t/2$ this equation can be transformed to the following expression, the **Mathieu-equation**:

$$\frac{d^2u}{d\xi^2} + (a_u - 2q_u \cos 2\xi)\mu \cdot u = 0 \tag{3.19}$$

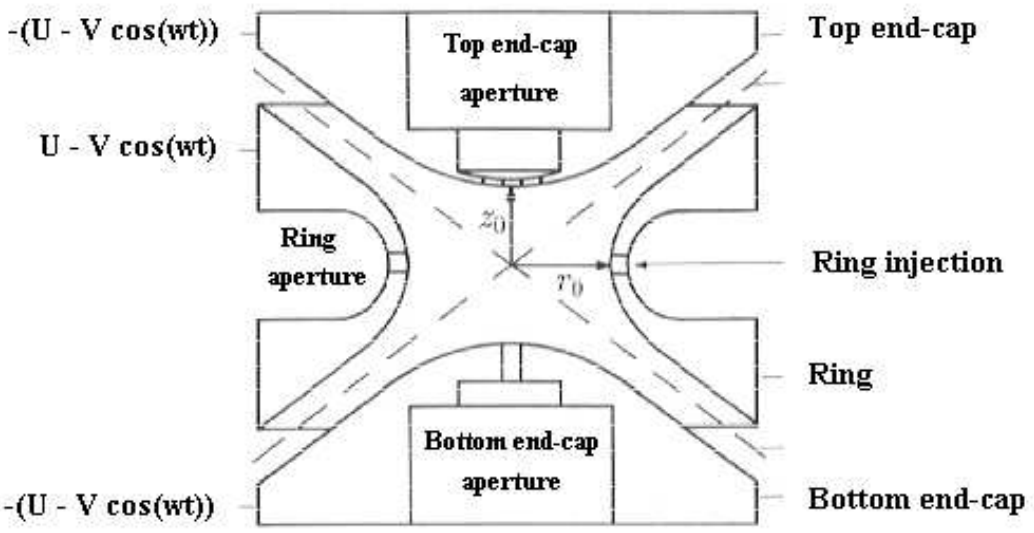

Figure 3.2: Principle structure of a Paul ion trap.

with u representing x, y or z, μ representing λ, σ or γ, respectively and

$$a_u = \frac{8eU}{mr_0^2\omega^2} \qquad and \qquad q_u = \frac{4eV}{mr_0^2\omega^2} \tag{3.20}$$

This equation was originally solved by Mathieu who was investigating the motions of a vibrating membrane. So the solutions are well known and can be found in literature, e.g. [Mathieu, 1868, McLachlan, 1947].

A three-dimensional quadrupole ion trap (see schematic **Figure 3.2**) is built of a hyperboloid ring electrode and two hyperboloid end-cap electrodes. The derivation of the formulas for the ion trap is analogue to the upper derivation but it is appropriate to solve the equations in cylindrical coordinates ($(x, y, z) \rightarrow (r, \theta, z)$; $x = r\cos\theta$, $y = r\sin\theta$, $z = z$). This leads to the following equations of motion:

$$\frac{d^2z}{dt^2} - \frac{4e}{mr_0^2}(U - V\cos\omega t)z = 0 \tag{3.21}$$

$$\frac{d^2r}{dt^2} + \frac{2e}{mr_0^2}(U - V\cos\omega t)r = 0 \tag{3.22}$$

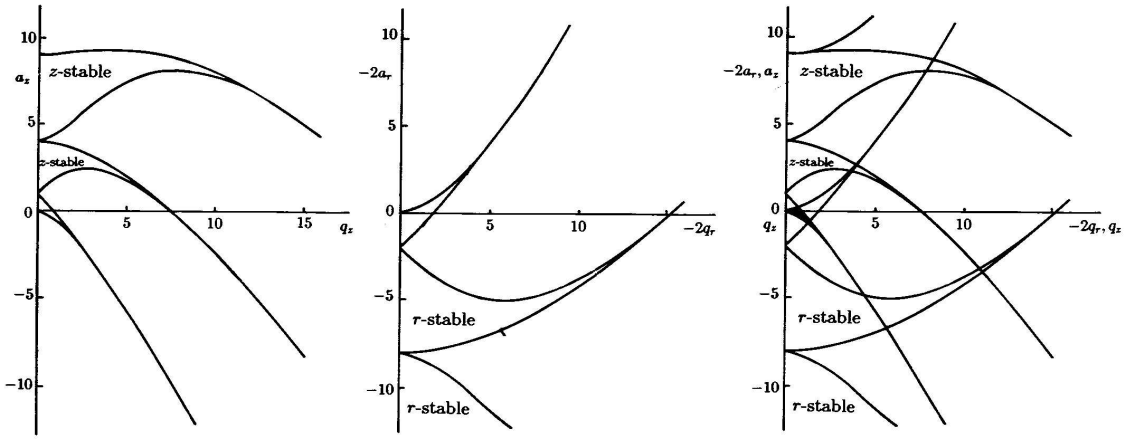

Figure 3.3: Graphical representation of stable solutions of the Mathieu equation for the three-dimensional quadrupole ion trap plotted in (a, q) space. Graphics by [March and Hughes, 1989].

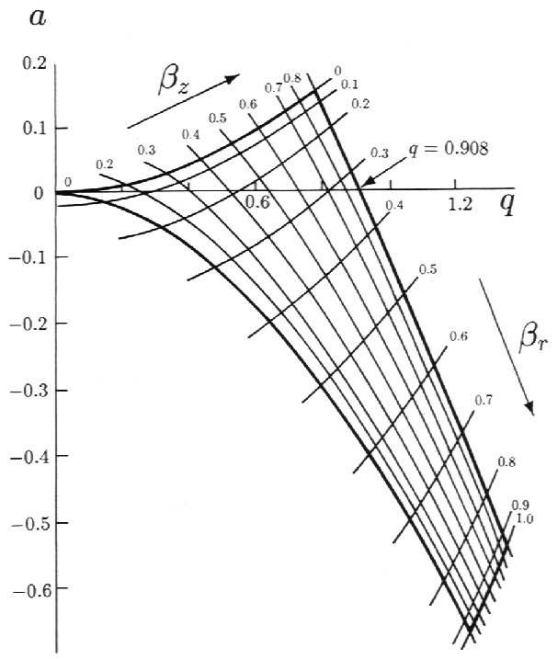

Figure 3.4: Stability region near the origin for the three-dimensional ion trap, plotted in (a, q) space [March and Hughes, 1989].

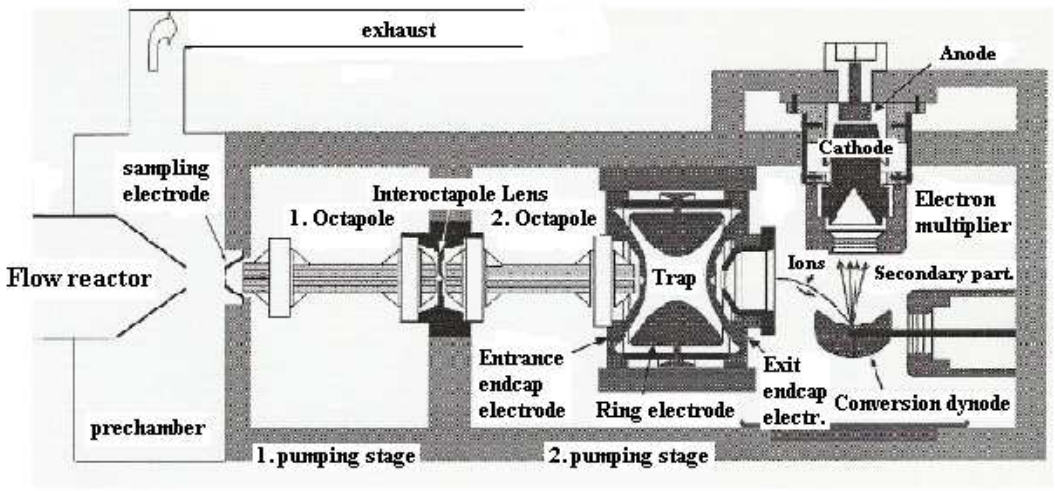

Figure 3.5: Schematic view of the structure of the IT-CIMS apparatus (Paul ion trap mass spectrometer PITMAS) [Hanke, 1999].

And with the substitutions $\xi = \omega t/2$ and

$$a_z = -2a_r = \frac{-16eU}{m\omega^2 r_0^2} \qquad and \qquad q_z = -2q_r = \frac{-8eV}{m\omega^2 r_0^2} \tag{3.23}$$

the Mathieu equation (3.19) is obtained again.

Furthermore, considering the boundary conditions $\phi(r_0, 0, 0) = \phi(0, r_0, 0) = \phi_0$ and $\phi(0, 0, z_0) = -\phi_0$ this leads to a condition for the physical shape of the trap:

$$r_0^2 = 2z_0^2 \tag{3.24}$$

Depending only on the two parameters a and q stable and unstable solutions of the Mathieu equations can be calculated, which determines if an ion can be kept inside the trap. A graphical representation of stable solutions is shown in **Figure 3.3** and the stability region near the origin can be seen in **Figure 3.4**.

A very good introduction to quadrupole storage mass spectrometry gives the book by R. March and R. Hughes [March and Hughes, 1989].

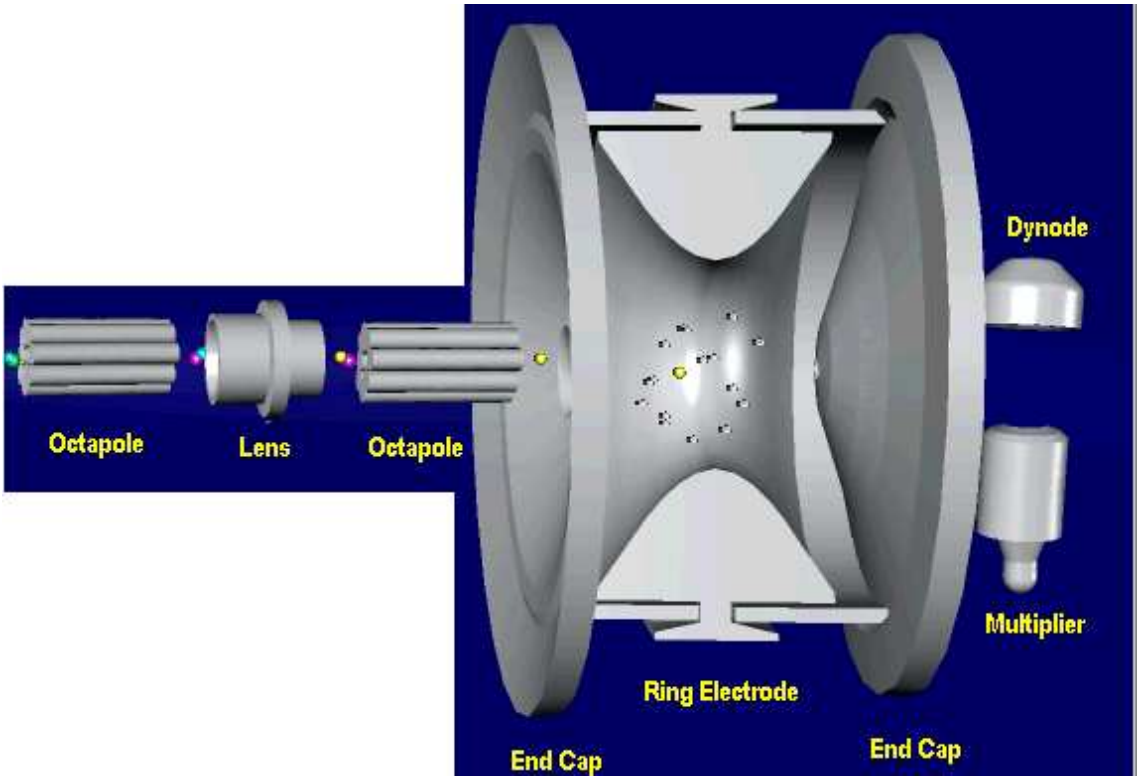

Figure 3.6: Three dimensional view of the ion optics, Paul trap and detection devices [graphics by Finnigan].

3.2.2 Ion Trap Mass Spectrometry (ITMS)

Our CIMS-apparatus is equipped with a commercial ion trap mass spectrometer (ITMS), made by Thermo Finnigan. The original instrument was constructed for the analysis of liquids (electro-spray). Our group changed the injection system to enable the analysis of gaseous compounds. **Figure 3.5** gives a schematic view of its interior. Through a critical front orifice (sampling electrode) the gas sample is soaked up by the spectrometer. Under operating conditions in the prechamber a pressure of about $4 \cdot 10^3$ Pa was measured, inside the spectrometer at the first pumping stage a pressure of about 10^{-1} Pa and at the second stage a pressure smaller than 10^{-3} Pa. On their way the ions first need to pass the ion optics, i.e. they are focussed by two octapoles and an inter-octapole lens, which have all positive potentials in case of negative ions and all negative potentials in case of positive ions (see **Figure 3.6**). Next, the ions are injected into the Paul trap through one of the

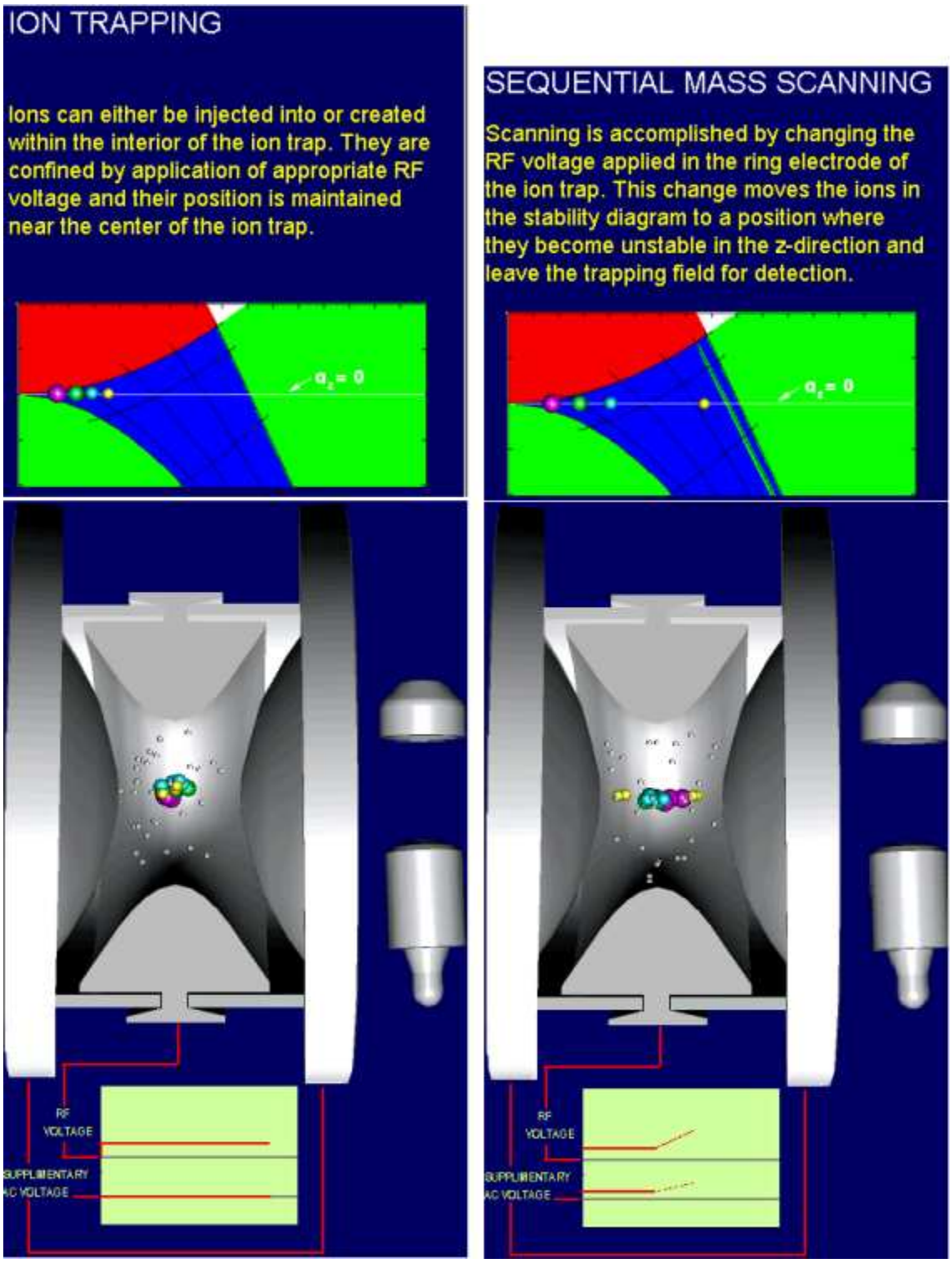

Figure 3.7: Mass storage (left) and selection (right) via change of the electrical potential in the trap. In the upper part the Mathieu stability diagram is shown [graphics by Finnigan].

end-cap electrodes for a certain time, which is called "injection time", and are stored there. The potential of the trap is kept in such a way, that all masses have stable orbits (**Figure 3.7**, left side). Inside the trap, helium is used as damping gas to slow down ("to cool") the ions and to displace molecules that could disturb the measurements like water. When a sufficient amount of ions is collected in the trap (this is guaranteed by a system which is called "Automatic Gain Control" (AGC)), the potential is changed in a way, that the orbits for one ion mass after each other become unstable in axial direction. Consequently, the ions are ejected successively from the trap, starting from the ions with the lowest mass (see **Figure 3.7**, right side). Finally, the ejected ions impinge on a conversion dynode and the electrons emitted by the dynode are counted via an electron multiplier.

The advantages of an ITMS compared to a linear QMS are the following: firstly the possibility to measure fast very low ion concentrations due to the ability of collecting and storing ions for a certain time in the trap and secondly the existence of a so-called "ion fragmentation mode". In this mode complex ions (large organic ions or cluster ions, e.g. $NO_3^-(HNO_3)_n$) can be excited via energetic collisions with helium and split up into their fragments, in the upper example into NO_3^- and n-times HNO_3. This method can especially be useful for investigations of chemical species with high molecular masses (e.g. volatile organic compounds), in which case usually for one mass value a wide range of possible substances exists. The composition of such compounds can be analyzed in the fragmentation mode and so it might be possible to determine the original substance.

Chapter 4

Project QUEST

The aim of the QUEST-project (Quantification of Aerosol Nucleation in the European Boundary Layer) is the qualitative and quantitative analysis of particle nucleation and growth in three different European regions: Boreal region, Coastal Atlantic region and Southern European region. The first of up to now three campaigns (QUEST 1) took place in Mace Head (Ireland, Coastal Atlantic region) in spring 2002, the second (QUEST 2) in Hyytiälä (Finland, continental boreal forest area) in spring 2003 and the third was split up between San Pietro Capofiume, Italy (QUEST 3a) and Heidelberg, Germany (QUEST 3b) in spring 2004 (both polluted continental regions). These places were chosen in order to cover nucleation events of all possible types in Europe: on the one hand, new particle formation basing on sea salt aerosols in a coastal, maritime region, on the other hand, nucleation events in continental regions, both in more or less clean air (Finland) and in polluted air (Italy and Germany). The main objectives of the QUEST project are both to understand the physical and chemical pathways that lead to new particle formation and to find out the meteorological conditions that are favored or even required during nucleation events. A further objective is to implement a European scale model that is able to predict the source strength of such events.

Within this work the focus will be on the campaigns in Hyytiälä and Heidelberg and a comparison of the results at these two measurement sites will be shown. During both the campaign in Hyytiälä (17th of March to the 13th of April 2003) and the Heidelberg-campaign (27th of February to the 4th of April 2004), besides many other parameters, sulphuric acid

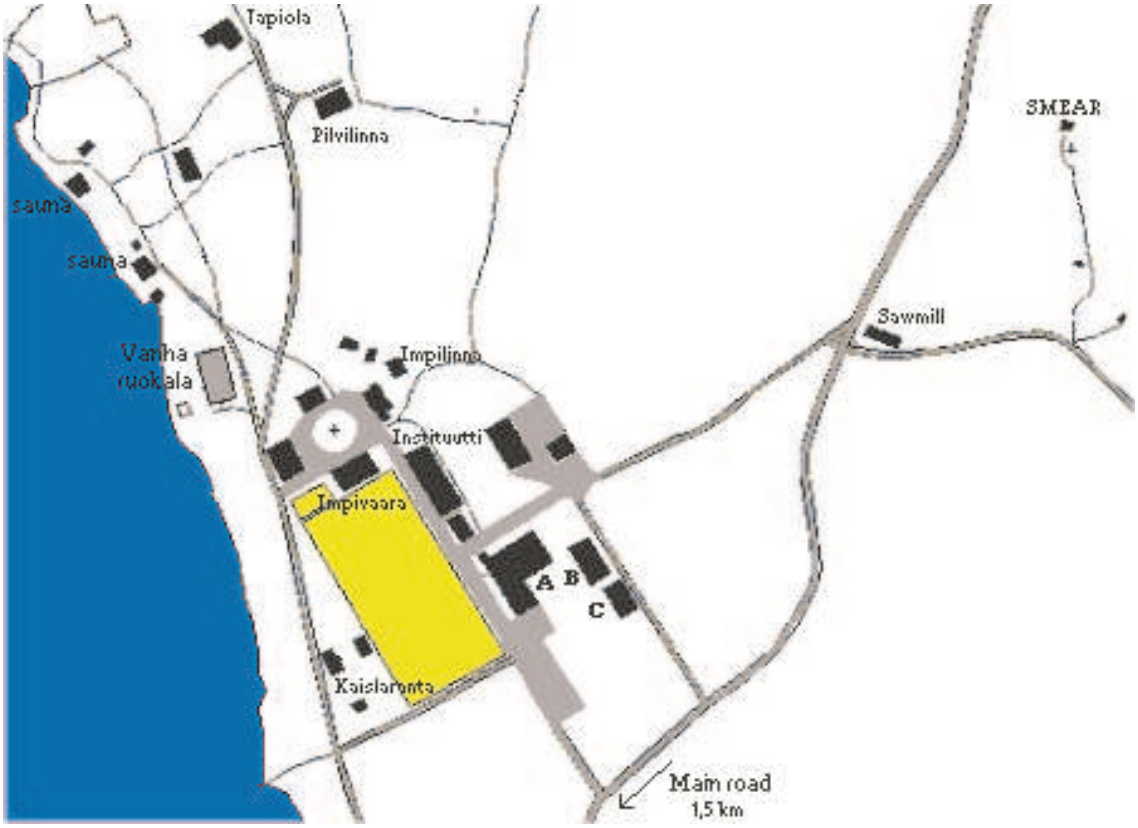

Figure 4.1: Site map of SMEAR II, the H_2SO_4-measurements were located near the sawmill.

concentrations and DMPS (Differential Mobility Particle Sizer) data were measured continuously on 21 and 38 days, respectively. From these data various quantities like growth, nucleation and source rates were calculated and compared for both sites.

4.1 Measurement sites

4.1.1 Hyytiälä

During QUEST 2 data were collected at the Station for Measuring Forest Ecosystem Atmosphere Relations (SMEAR II) in Hyytiälä, Finland. The station is located in Southern Finland ($61°51'N, 24°17'E$, 181 m asl[1]), with extended areas of Scots Pine (Pinus sylvestris) dominated forests, see **Figure 4.1** and maps in the appendix A.1 and A.2. The conditions at the site are typical for a background location, which means that no anthropogenic

[1] above sea level

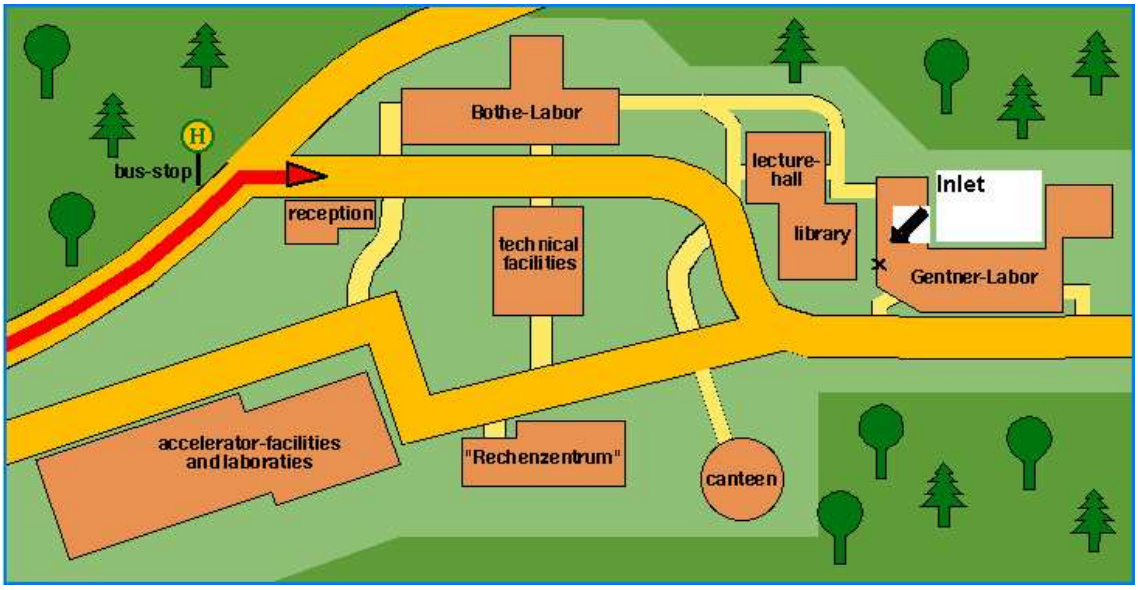

Figure 4.2: Site map of the MPI-K, our laboratory is marked by a cross.

pollution sources are nearby. However, measurements were occasionally polluted by the station buildings (0.5 km away) and the city of Tampere (60 km away), both located in a west-south-west direction (215 - 265 degree) from the instruments. In the framework of this thesis measurements of H_2SO_4, temperature, humidity, wind-direction, particle number concentration and size distribution were taken into account. For a more detailed description of SMEAR II and instrumentation, I would like to refer to [Kulmala et al., 2001] and www.honeybee.helsinki.fi/smear/.

4.1.2 Heidelberg

Data were collected at the MPI-K Heidelberg (Max-Planck-Institute for Nuclear Physics), Germany ($49°23'N, 08°41'E$, 350 m asl) about 4 km southeastwards of Heidelberg and 200 m above the city within deciduous forest area (beech, maple, chestnut, birch, oak), see **Figure 4.2** and overview maps in appendix A.3 and A.4. In about 0.5 km distance from the MPI a farmhouse and a rehabilitation center are located. In the east Heidelberg is surrounded by hilly forest area (Odenwald). In the west Heidelberg borders on the Rhine valley, where large cities (Mannheim, Ludwigshafen, Karlsruhe) with various industrial complexes and also power

stations are settled. This region is one of the most polluted areas in Germany. During QUEST 3b measurements of H_2SO_4, solar radiation, temperature, humidity, wind direction/speed and particle data (DMPS) were carried out. The DMPS system was provided by the Leibniz Institute for Tropospheric Research (Leipzig, Germany). The additional meteorological data were measured using a standard weather station with wind measurements on the roof of MPI-K.

Chapter 5

Experimental Setup and Calibration

In this chapter the experimental setup for the measurement of sulphuric acid concentrations during QUEST 3b will be described. The description of the calibration procedure applied will be particularly emphasized .

5.1 Experimental Setup

The principle setup used in Hyytiälä during the QUEST 2 campaign has already been described by Scholz [Scholz, 2004]. Some modifications due to the different conditions at the measurement site Heidelberg were needed (e.g. the inlet was completely horizontal) and can be seen in **Figure 5.1**. In this section the modifications of the setup for QUEST 3b will be mentioned.

5.1.1 Inlet System and Flow Reactor

In order to keep the losses of sulphuric acid to the walls of the measurement devices as low as possible, the inlet system needs to be as short as possible. However, it is also important to construct the inlet outside the measurement station long enough to measure air that was not yet in contact with the walls of the building. During QUEST 3b this was realized by a tube of 4 cm in diameter inside a tube of 20 cm in diameter. The length values chosen during QUEST 3b can also be seen in **Figure 5.1**. The inlet side of the flow reactor (KF40-tube) was closed by a so-called ion cone with an aperture of 6 mm, the PITMAS side by a critical

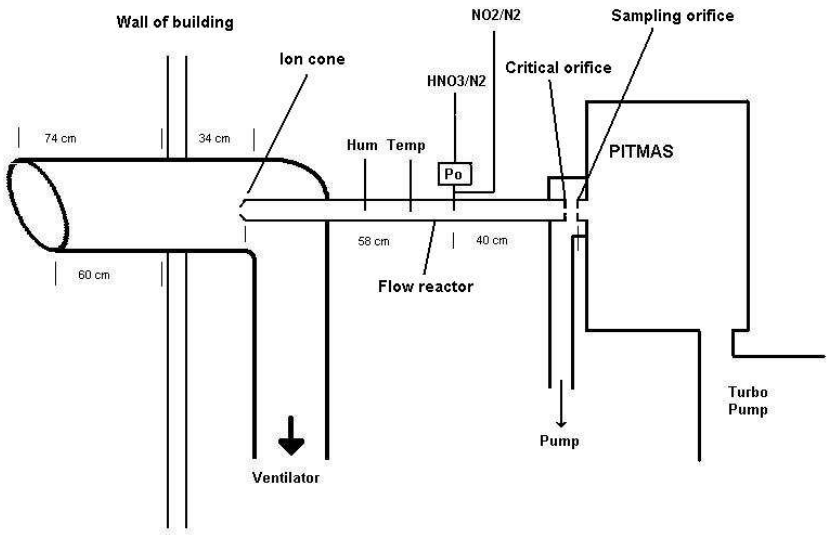

Figure 5.1: Schematic view of the experimental setup: Inlet system with ventilation (left), flow reactor with sensors and Polonium ion source (middle), PITMAS (right).

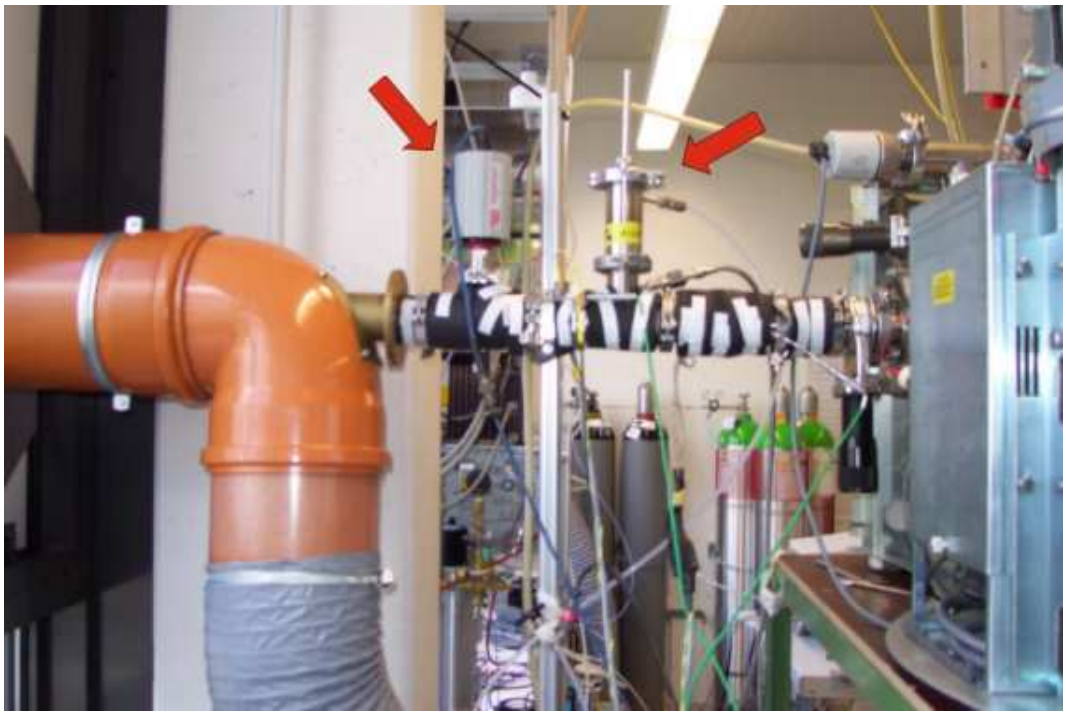

Figure 5.2: Picture of the flow reactor with sensors (left arrow) and ion source (right arrow).

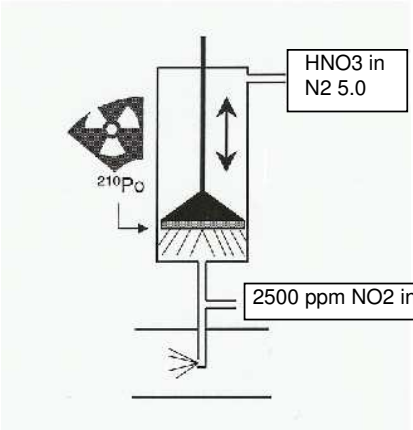

Figure 5.3: Schematic view of the Polonium ion source, 3 slm (standard liters per minute) HNO_3 in N_2 and 1.5 slm NO_2 in N_2 were added.

orifice of 1.5 mm in diameter. The front plate of the PITMAS had a sampling orifice of 0.15 mm in diameter. Inside the flow reactor atmospheric pressure and downstream of the critical orifice a pressure of $4{\cdot}10^3$ Pa was measured. The ventilation system produced an air flow of 10^3 slm (standard liters per minute) and the flow reactor pump generated a flow through the critical orifice of 20 slm. The flow reactor was heated to a temperature of 17 - 20°C in order to have constant measurement conditions.

The educt ions $NO_3^-(HNO_3)_n$ were produced in a Polonium α-source (activity 185 MBq in March 2004, half-life 138.4 d, see **Figure 5.3**). This source is specifically suitable because of its very clean product ion spectrum as opposed to the often used glow-discharge ion sources. The source was originally developed by Hanke ("α-bombardment ionization capillary tube ion source, *αbcis*", [Hanke, 1999]). In our case, 3 slm HNO_3 in N_2 of purity 5.0 were used as source gas[1] and 1.5 slm NO_2 in N_2(2500 ppmv) were added straight after the source. This NO_2 has two functions. Firstly, it produces $NO_3^-(HNO_3)_n$ ions. Secondly, and this is the more important factor, it is used as so-called quench-gas: NO_2 reacts with OH radicals which are also produced by the ion source and which would otherwise react with atmospheric SO_2 resulting in an artificial H_2SO_4-signal. By adding NO_2 this artificial H_2SO_4-signal is suppressed. With the flow of 20 slm and a distance of 40 cm between ion source and spec-

[1]The gas mixture was produced in a permeation oven with a permeation tube by Dynacal and had a volume mixing ratio of 100ppbv.

trometer, we got an ion residence time in the flow reactor of about 1 s. After this time, the ions were sampled by the sampling orifice of the ITMS and the ratio of product and educt ions was measured. All values during PITMAS operation (e.g. the applied voltages to the ion optics) were recorded with the software TUNE PLUS (Finnigan). A so-called HEADER, which indicates all the corresponding values, is stored for each spectrum. An example for a HEADER with usual values during operation and typical spectra during normal operation and during calibration can be found in the appendix.

5.1.2 Additional Data

All other data, like those obtained from flow controllers, temperature sensors and dew point sensors were recorded via a pulse code modulation (PCM) system, which is described in more detail by Aufmhoff in [Aufmhoff, 2004].

Additional meteorological data was acquired by a commercial weather station (WM 918 by Huger Electronics) with wind measurements on the roof of the MPI-K and recorded via the software SBWeather. A light sensor for measurements of solar radiation was installed on the roof as well.

5.2 Calibration

The calibration source was originally built up by Reimann [Reimann, 2000] for calibration of OH-, HO_2- and RO_2-radicals. In his thesis a detailed description can be found and therefore at this point the focus will be on the principles and the calculation of the calibration factor during our measurements. All formulas are taken from [Reimann, 2000].

The calibration is based on the artificial production of OH-radicals through the photolytic dissociation of water.

$$H_2O + h\nu \longrightarrow H + OH \qquad \lambda < 185\text{nm} \tag{5.1}$$

These OH-radicals can further react with the added SO_2 (surplus) and form H_2SO_4. If the reaction time is long enough ($> 10^{-3}$ s) all OH-radicals will react. Since one OH forms exactly one H_2SO_4-molecule, only the OH-concentration needs to be determined to know the

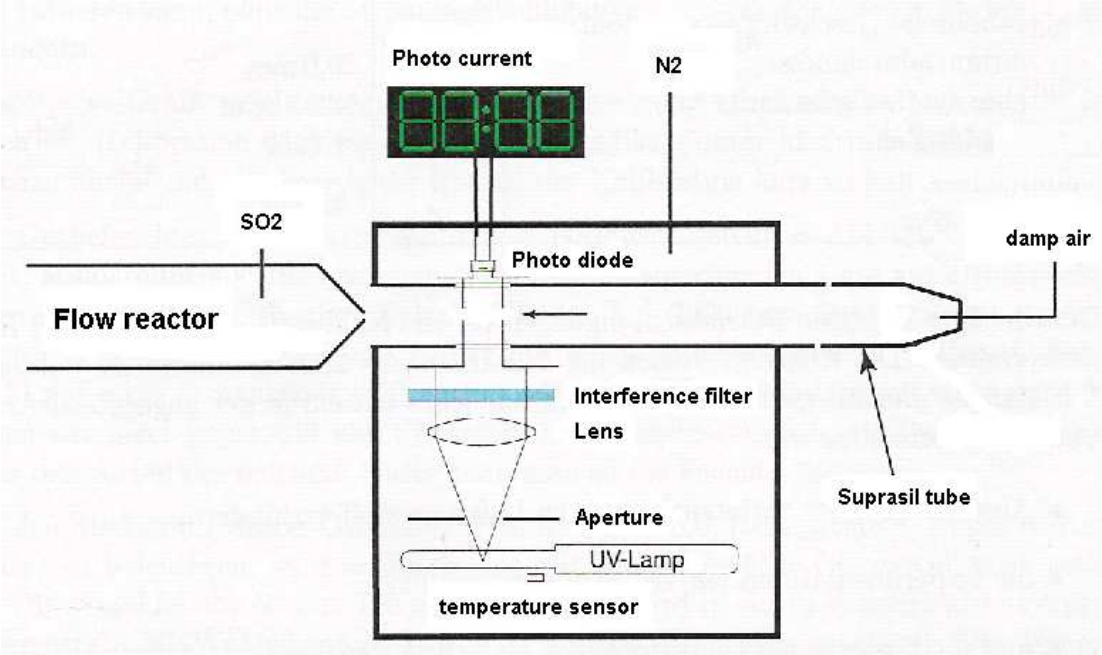

Figure 5.4: Schematic view of the calibration setup, calibration source with UV-lamp, photo diode, suprasil tube; flow reactor (left) with SO_2-injection.

H_2SO_4-concentration as well. The OH-concentration [OH] can be calculated from

$$[\mathrm{OH}] = [\mathrm{H_2O}]_0 \, \sigma_{\mathrm{H_2O}} \, \Phi_{\mathrm{OH}} \, \Psi \, \tau \tag{5.2}$$

where $[H_2O]_0$ represents the water vapor concentration, σ_{H_20} the photo dissociation cross section of water at 185 nm, Φ_{OH} the quantum yield, Ψ the photon flux and τ the irradiation time.

The principal setup can be seen in **Figure 5.4**. Humid air is passed through a suprasil tube and inside the source irradiated by UV-light, the photo current is measured via a photo diode. The OH radicals are then soaked up by the flow reactor and react with the added SO_2.

5.2.1 Calculation of the Calibration Factor

Now the OH-concentration can be calculated building on known parameters.

The *water vapor concentration* is

$$[\mathrm{H_2O}]_0 = \frac{p_{H_2O}}{p_0} \cdot \frac{T_0}{T_{sr}} \cdot \frac{N_A}{V_0} \tag{5.3}$$

so with

p_{H_2O}	=	600 Pa $\pm 14\%$	Water Vapor Partial Pressure[2]
T_0	=	273.15 K	Standard temperature
N_A	=	$6.022045 \cdot 10^{23}$ mol^{-1}	Avogadro constant
p_0	=	$1.01325 \cdot 10^5$ Pa	Standard pressure
T_{sr}	=	301.95 K	Flow reactor temperature
V_0	=	$2.241383 \cdot 10^{-2}$ m^{3}mol^{-1}	Standard volume

we get

$$[\mathrm{H_2O}]_0 \approx 1.4 \cdot 10^{23}\ m^{-3} \tag{5.4}$$

The *absorption cross section of water* at 185 nm is

$$\sigma_{\mathrm{H_2O}} = 7.14 \cdot 10^{-24}\ m^2 \tag{5.5}$$

The *quantum yield* is

$$\Phi_{\mathrm{OH}} = 1.0 \pm 1\% \tag{5.6}$$

The *photon flux* is

$$\Psi = \frac{I\lambda}{sAhc} \cdot k_d \cdot k_t \cdot (e^{k_\sigma} + \rho \cdot e^{-k_\sigma}) \tag{5.7}$$

with

$$k_\sigma = (\sigma_{O_2}[\mathrm{O_2}] + \sigma_{H_2O}[\mathrm{H_2O}]_0) \cdot R \tag{5.8}$$

[2]Calculated with approximation (7.16) in [Reimann, 2000].

and with the following measured values and constants

I	=	$4.45 \cdot 10^{-8}$ A $\pm 5.6\%$	Photocurrent
λ	=	$1.849 \cdot 10^{-7}$ m	Wavelength
s	=	0.097 A/W $\pm 2.7\%$	Spectral sensitivity
A	=	$1.3 \cdot 10^{-5}$ m^2	Sensitive surface area of the photodiode
h	=	$6.626 \cdot 10^{-34}$ Js	Planck-constant
c	=	$2.998 \cdot 10^{8}$ m/s	Light velocity
k_d	=	$1.380 \pm 1.4\%$	Correction factor for beam divergency
k_t	=	$1.293 \pm 0.8\%$	Correction factor for transmissivity
ρ	=	$0.085 \pm 1.4\%$	Reflection ability
σ_{O_2}	=	$1.4 \cdot 10^{-24}$ m$^2 \pm 22\%$	Absorption coefficient of O_2 at $\lambda = 185$ nm
σ_{H_2O}	=	$7.14 \cdot 10^{-24}$ m$^2 \pm 2.8\%$	Absorption coefficient of H_2O at $\lambda = 185$ nm
$[O_2]$	=	$5.0 \cdot 10^{24}$m^{-3}	Oxygen concentration in suprasil tube ($0.2 \cdot pN_A/RT$)
$[H_2O]_0$	=	$2.0 \cdot 10^{23}$m^{-3}	Water vapor concentration from above
R	=	0.01 m	Radius of the suprasil tube

we get

$$\Psi \approx 6.7 \cdot 10^{16}\ s^{-1}m^{-2} \tag{5.9}$$

as a value for the photon flux.

The *irradiation time* is

$$\tau = \frac{k_l\, b\, p_{sr}}{\chi_r\, p_0} \cdot \frac{T_0}{T_{sr}} \cdot \pi R^2 \cdot \left(1 - \sqrt{1 - \frac{\chi_r}{\chi_R}}\right) \tag{5.10}$$

with the values

k_l	=	$1.078 \pm 5\%$	Correction factor for the length of the irradiation zone
b	=	0.015 m	Aperture width
p_{sr}	=	$9.70 \cdot 10^4$ Pa $\pm 0.2\%$	Pressure in the suprasil tube
χ_r	=	15 slm $\pm 10\%$	Flux soaked up by the flow reactor
χ_R	=	$19.5 - 19.8$ slm $\pm 1\%$	Total flux in the suprasil tube

we obtain

$$\tau \approx 9 \cdot 10^{-3} s \tag{5.11}$$

Now with the equations (5.3) to (5.10) equation (5.2) can be solved yielding a sulphuric acid concentration of

$$[H_2SO_4] = [OH] = 5 \cdot 10^{14} \text{ m}^{-3} \pm 20\% \tag{5.12}$$

and considering the calibration factor CF= $[H_2SO_4]/ln(1 + R)$ with R measured we obtain

Calibration Factor $$\text{CF} = 2.11 \cdot 10^{15} \text{ m}^{-3} \pm 20\% \tag{5.13}$$

This factor was used in the evaluation of the sulphuric acid measurements. The proportionality factor from the ACIMS-Formula $1/(k \cdot t)$ was determined as a rough estimation (as many parameters and conditions are not considered) yielding

$$\text{CF}_{\text{ACIMS}} = 0.7 \cdot 10^{15} \text{ m}^{-3} \tag{5.14}$$

Hence comparing to the theoretically calibration factor one obtains $\text{CF}/\text{CF}_{\text{ACIMS}} = 3$. If the dilute gas flow (HNO_3, NO_2 and SO_2 are added in the flow reactor) is considered for ACIMS, the ratio ranges around 2.3.

Chapter 6

Measurements

In the previous chapter the calibration factor for the sulphuric acid measurements in Heidelberg was given. Now further factors that have to be considered with regard to the concentration calculations will be mentioned and the measured data will be presented.

6.1 Additional Considerations

The ratio R of product to educt ions was in practice the ratio of measured $HSO_4^-(HNO_3)$ (mass 160) to measured $NO_3^-(HNO_3)$ (mass 125). Only these two mass lines were taken into account as they are the dominant lines and the mass lines of clusters with 0 or more than 1 nitric acid molecules can be neglected [Uecker, 2002]. This ratio R was afterwards corrected according to the background signal of the measurement device, which was regularly determined during the campaign. The basic principle, sulphuric acid absorption on a filter with several layers of laboratory paper, has also already been described in [Scholz, 2004]. In our case as a consequence of these background measurements the detection limit was in the range of $3 \cdot 10^5$ cm^{-3}. Results of background measurements are presented in **Figure 6.1**. In this context it is important that the background value was constant in time and independent of the educt ion concentration (with exception of the 7th of March). This justifies that only the measured concentrations of the product mass 160 were corrected by the background values. The fact that the background signal is independent of the educt ion concentration indicates, that artificially created H_2SO_4 is only a secondary reason for the background. Otherwise, the more educt ions also the more product ions should be created. The independence is a clear

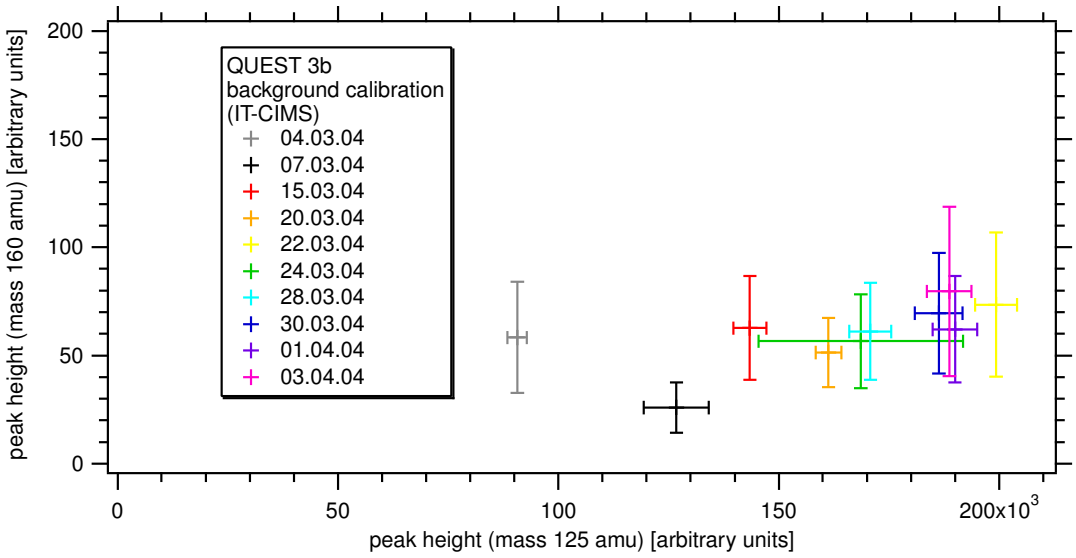

Figure 6.1: Measurements of the background: Plotted is the background value of the mass line 160 ($HSO_4^-(HNO_3)$) versus mass line 125 ($NO_3^-(HNO_3)$) in arbitrary units.

hint that the background is at least partly caused by electronic noise or by artificial H_2SO_4-creation inside the trap. If it was possible to reduce this instrumentally caused background, it should be possible to reach an even smaller detection limit.

The relative error of the H_2SO_4-concentration was determined to be ±30 %. This error is composed of the systematical and statistical error of the calibration factor, which was all together ±20 % and a statistical error of the concentration measurements of about ±10 %[1].

6.2 Measured Sulphuric Acid Concentrations

On the following pages the measured sulphuric acid concentrations during QUEST 3b (27th of February to 4th of April 2004) are shown (**Figures 6.2 and 6.3**). The concentrations are corrected according to the background mentioned above. Time gaps in the graphs are caused either by background measurements, maintenance or simply by bad weather conditions.

On almost all days, concentrations of at least 10 times above the detection limit were

[1]The count rate ranged usually around 100 (arbitrary units), the statistical error is consequently $\sqrt{100}$, which corresponds to 10 %

measured with exception of week two, which was an extremely wet and rainy week. Therefore the atmospheric H_2SO_4-concentration was very low. In the following chapters further analysis of these concentrations will be embedded in the comparative analysis of the data from Hyytiälä and Heidelberg.

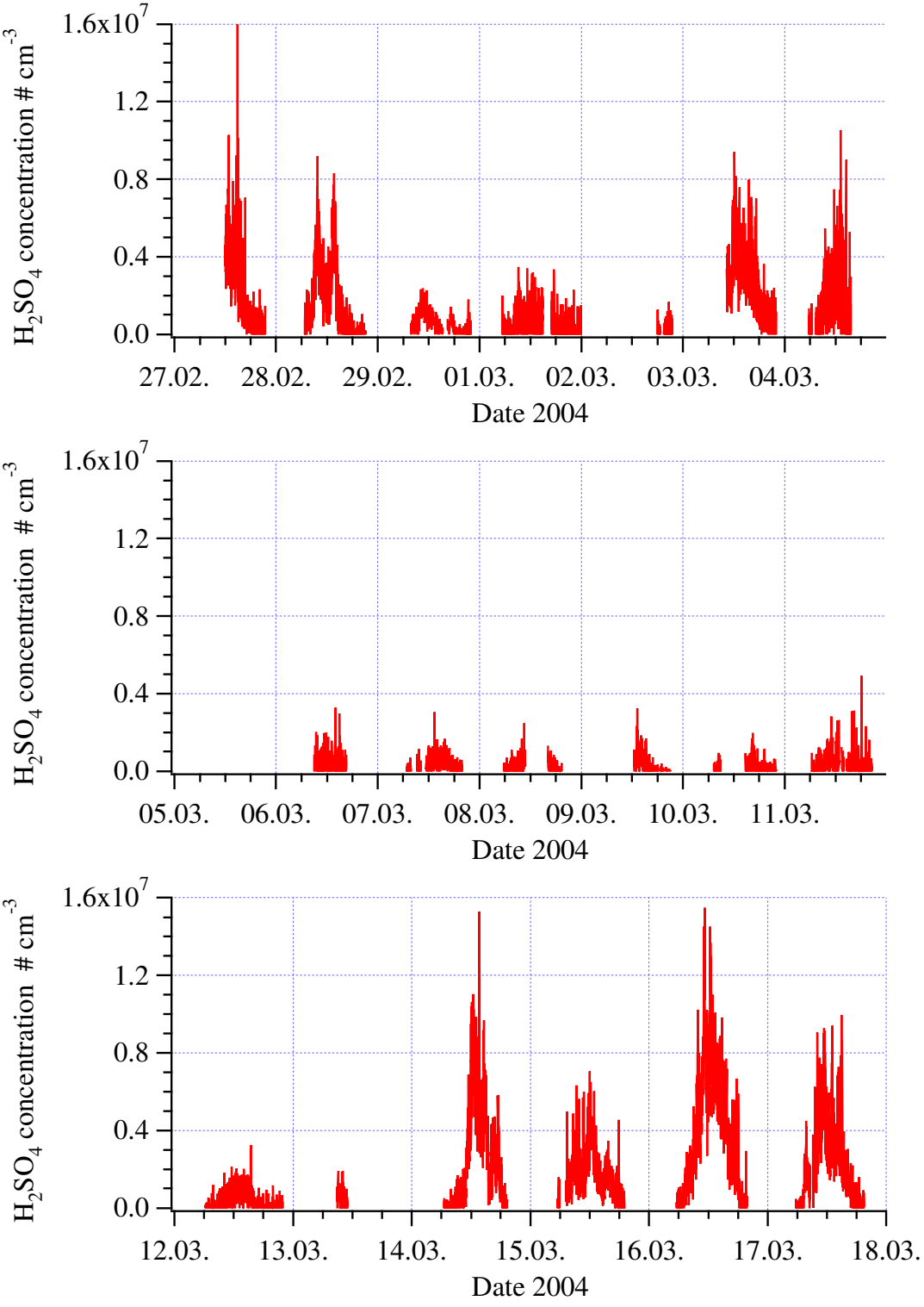

Figure 6.2: Overview of the measured sulphuric acid concentrations during QUEST 3b Heidelberg, February 27th till March 17th.

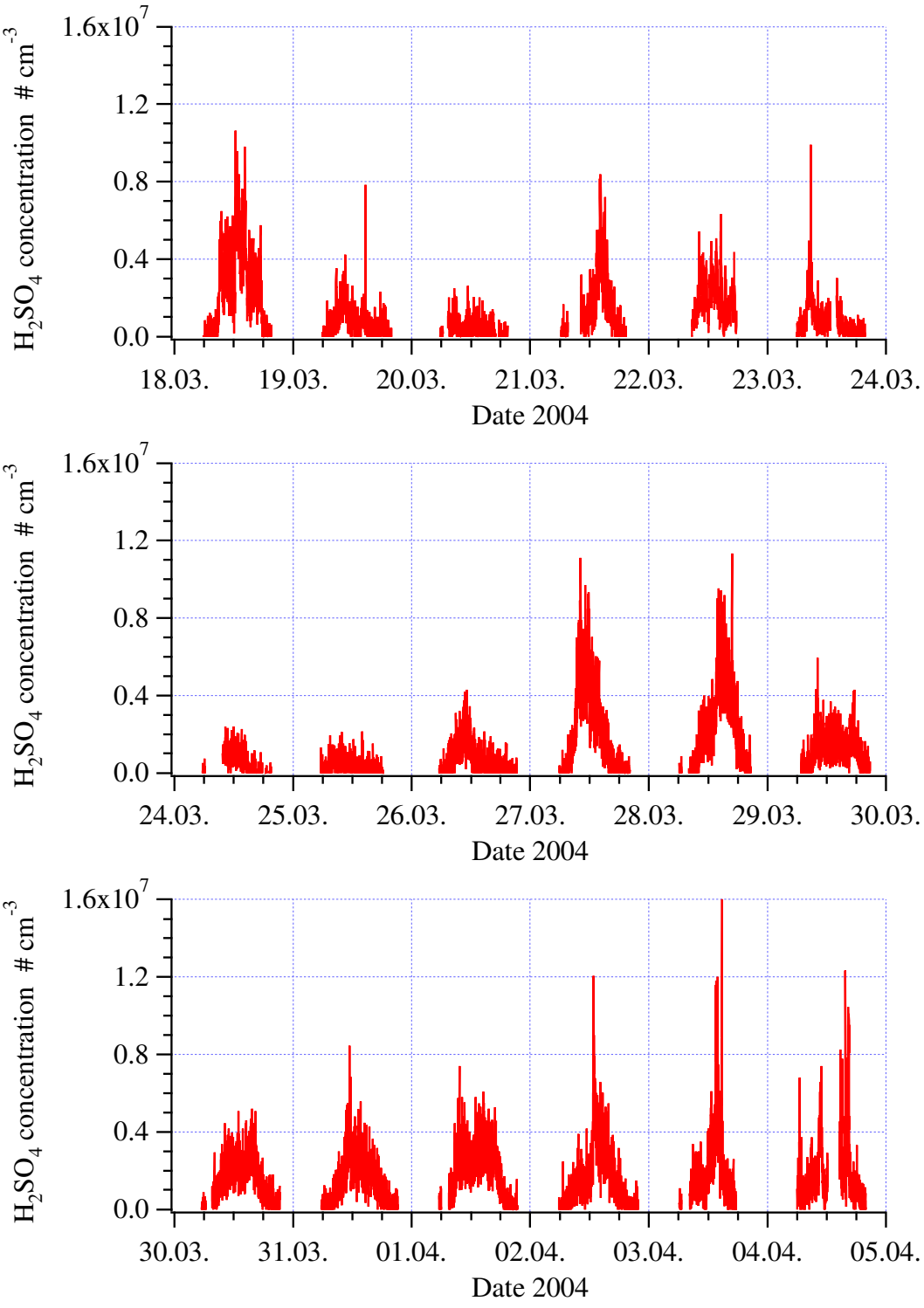

Figure 6.3: Continuation of the overview, March 18th till April 4th.

Chapter 7

Data Analysis

This chapter will deal with the methods that were used to analyze particle formation events in Hyytiälä and Heidelberg and the role sulphuric acid plays in the formation and growth of new particles. In the first section some important parameters that were calculated from DMPS data will be defined. In the following part, all *measured* data will be presented in comparison for both measurement sites.

7.1 Definitions

The Differential Mobility Particle Sizer (DMPS) yields the number concentrations of particles between 3 and 800 nm diameter, divided in 40 different size bins (or size classes), for 15 minutes time intervals. In **Figure 7.1** the DMPS plot of a typical new particle formation (nucleation) event can be seen. High amounts of small particles from a size of 3 nm up to 10 nm starting at 2 pm were measured.
From these data various parameters were calculated.

7.1.1 Condensation Sink

The aerosol *condensation sink* (CS) determines how rapidly molecules will collide with pre-existing aerosols [Kulmala et al., 2001] and can be calculated from

$$\mathrm{CS} = 4\pi D \int_0^\infty r\beta_M(r)n(r)dr = 4\pi D \sum_i \beta_M r_i N_i \tag{7.1}$$

with D being the diffusion coefficient (in our case the diffusion coefficient of sulphuric acid), β_M the transitional correction factor typically calculated using the expression by

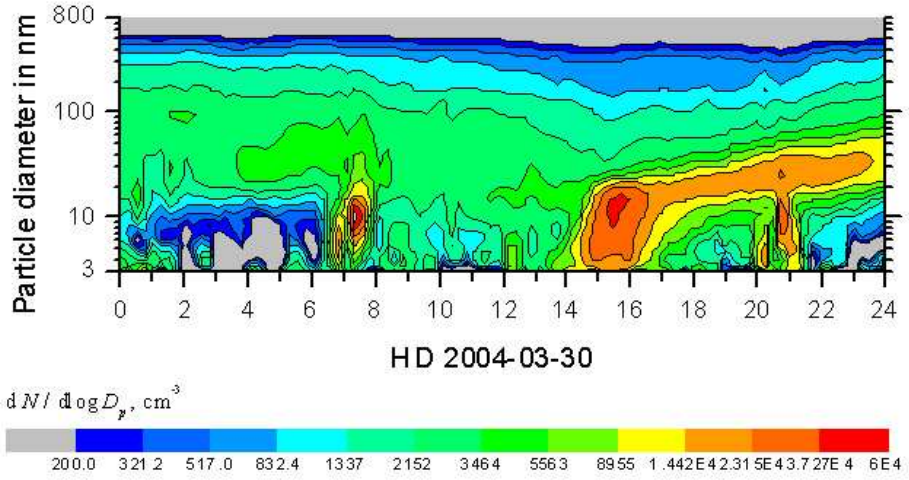

Figure 7.1: Typical new particle formation event, recorded on the 30th of March 2004 in Heidelberg. Plotted is the particle diameter versus time, the particle number concentration as color code.

[Fuchs and Sutugin, 1971] (see equation 2.12), N_i and r_i are the number concentration and the radius of the particles in the i'*th* size class measured with a DMPS system at dry relative humidity. The dimension of CS is s^{-1} and it can be interpreted as the inverse lifetime of the particles.

7.1.2 Growth Rate

Growth rates were calculated in two different ways. The first method was to obtain a total growth rate for the whole event from the particle number concentrations between 3 and 25 nm diameter from DMPS plots on days where a clear nucleation event was observed (this growth rate is called GR1). To reduce statistical errors the time of the highest concentration value in each size class was determined by fitting a lognormal distribution to the particle concentration. From these values a growth rate in nm h^{-1} could be calculated.

Secondly a so-called "timeshift" analysis was used, which compares the shape of two curves - sulphuric acid and the particle number concentration between 3 and 6 nm (N3). This method has to be explained a bit more in detail. In **Figure 7.2** the number concentration of

Figure 7.2: Comparison of the N3-curve (green line) and H_2SO_4-curve (red line) on the 25th of March 2003 in Hyytiälä. The time lag which was used in the calculations of growth rate 2 is marked by a black bar.

the smallest detectable particles N3 and the sulphuric acid concentration are plotted versus time for one example day in Hyytiälä. The shape of the N3 curve usually follows the H_2SO_4 curve with a certain time lag as sulphuric acid is the main precursor gas known so far for new particle formation. The time lag is due to the fact that new particle formation starts with particles of approximately 1 nm diameter but the DMPS system can only detect particles of at least 3 nm diameter, whose formation from 1 nm particles requires a certain growth time. Consequently this time lag, determined from the time difference between the first two slopes (marked in the graphic by a black bar), is the time span required for the first 2 nm growth. The growth rate GR2 for the initial 2 nm growth was determined in this way.

7.1.3 Particle Formation Rate

The *particle formation rate* J was determined from the total concentration of particles with diameters smaller than 25 nm. The formation rate ($\Delta concentration/\Delta t$) in $cm^{-3}s^{-1}$ was

calculated for a time interval starting when the particle concentration started to increase and ending at its maximum value [Kulmala et al., 2004b].

7.1.4 Condensable Vapor and Source Rate

The *condensable vapor concentration* C_{vap} is a property for the expected amount of vapor that is necessary to enable new particle formation and a certain growth rate. If the growth rate of the particles is known, C_{vap} can be integrated following [Kulmala, 1988]. In the size region of new, nanometer-size particles the result is a linear function of the growth rate GR

$$C_{vap} = 1.37 \cdot 10^7 \text{ cm}^{-3} \cdot GR \tag{7.2}$$

where the GR is given in nm/h.
Using this we can estimate a source rate Q of this vapor. According to [Kulmala et al., 2001] we obtain for the condensable vapor concentration

$$\frac{dC_{vap}}{dt} = Q - CS \cdot C_{vap} \tag{7.3}$$

Now if we assume steady state

$$\frac{dC_{vap}}{dt} = 0 \tag{7.4}$$

we get

$$Q = CS \cdot C_{vap} \tag{7.5}$$

as a value for the *source rate of the condensable vapor.*

7.2 Measured data

All together there was a total number of 19 nucleation events in Hyytiälä and 10 in Heidelberg of which 8 in Hyytiälä (3 in Heidelberg) were classified class 1, 6 (3) class 2 and 5 (4) belonged to class 3. The classification goes as follows: Class 1 means a clear formation of new 3 nm particles and their following extended growth as it can be seen in Figure 7.1, class 2 means clear formation but the growth is less pronounced and class 3 means that there is some formation but no or only very poor growth is visible [Mäkelä et al., 2000, Boy and Kulmala, 2002].

The concentration of preexistent background aerosol (mainly particles between 10 and 300 nm in diameter) was always slightly higher in Heidelberg than in Hyytiälä but at both sites a strong decline of the background particle concentration before events could be observed for most event days. In those cases the total particle number concentration was below 7000 cm^{-3} in Hyytiälä and below 10000 cm^{-3} in Heidelberg whereas it reached usually around 15000 cm^{-3} at both places during daytime. This is a well known result because otherwise the condensable vapors would condense onto the preexistent particles and would not be available for nucleation.

Figure 7.3 and **Figure 7.4** show the measured sulphuric acid concentration and the calculated condensation sink in Hyytiälä and Heidelberg, respectively. The concentrations of sulphuric acid were in the same range ($2 \cdot 10^6 - 16 \cdot 10^6$ cm^{-3}), but the mean was somewhat higher in Heidelberg ($6 \cdot 10^6$ cm^{-3}) compared to Hyytiälä ($4 \cdot 10^6$ cm^{-3}). The values of the condensation sink range from 0.005 to 0.03 s^{-1} in Heidelberg and from 0.0005 to 0.007 s^{-1} in Hyytiälä. Moreover, the variation was much higher in Heidelberg, especially during daytime. We also would expect these approximately 10 times higher CS-values in Heidelberg compared to Hyytiälä because of the higher degree of pollution in Heidelberg. Furthermore the variations in Heidelberg reflect the influence of anthropogenic pollution sources, particularly industry, traffic and heating of houses.

In **Figure 7.5** and **Figure 7.6** solar radiation and temperature during both campaigns are shown. In Hyytiälä specifically UV-B radiation (wavelength < 320 nm) was measured by use of a UV-B sensor; in Heidelberg a Lux sensor was used with a sensitivity maximum between 500 and 600 nm wavelength. This is the reason for the up to 40 times higher radiation values in Heidelberg. UV-B radiation with wavelengths smaller than 310 nm is responsible for the formation of $O(^1D)$ via the photolysis of ozone, so this is the most interesting wavelength section with regard to sulphuric acid formation. Yet the diurnal variation of the UV-B radiation follows the visible light, with exception of early morning and late evening, when due to the longer path through the atmosphere especially short wavelengths are filtered out of the solar spectrum. Consequently, the diurnal variation of UV-B radiation can be estimated from the total radiation.

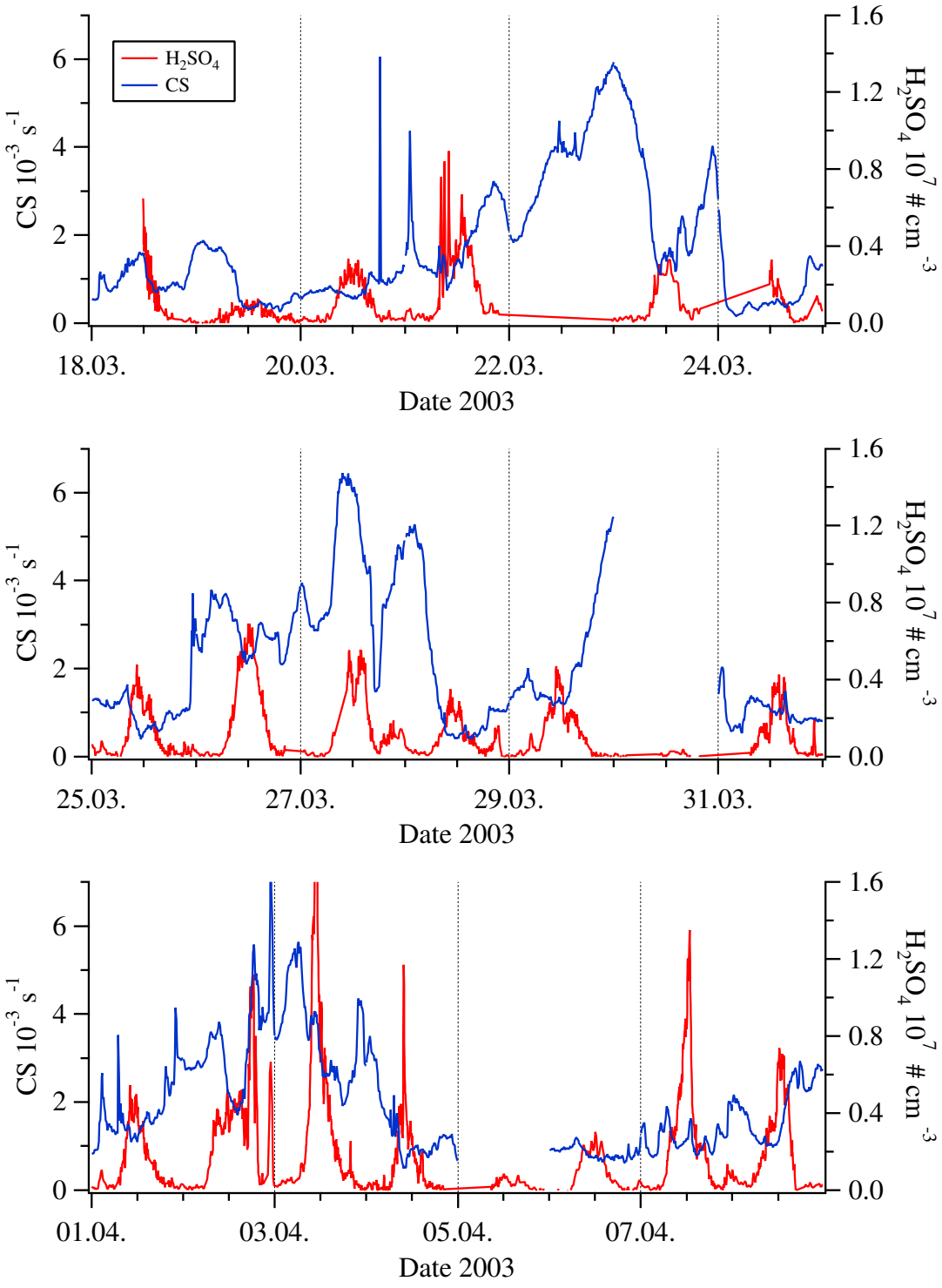

Figure 7.3: Hyytiälä: H_2SO_4-concentrations (red line) and Condensation Sink (blue line) versus Time.

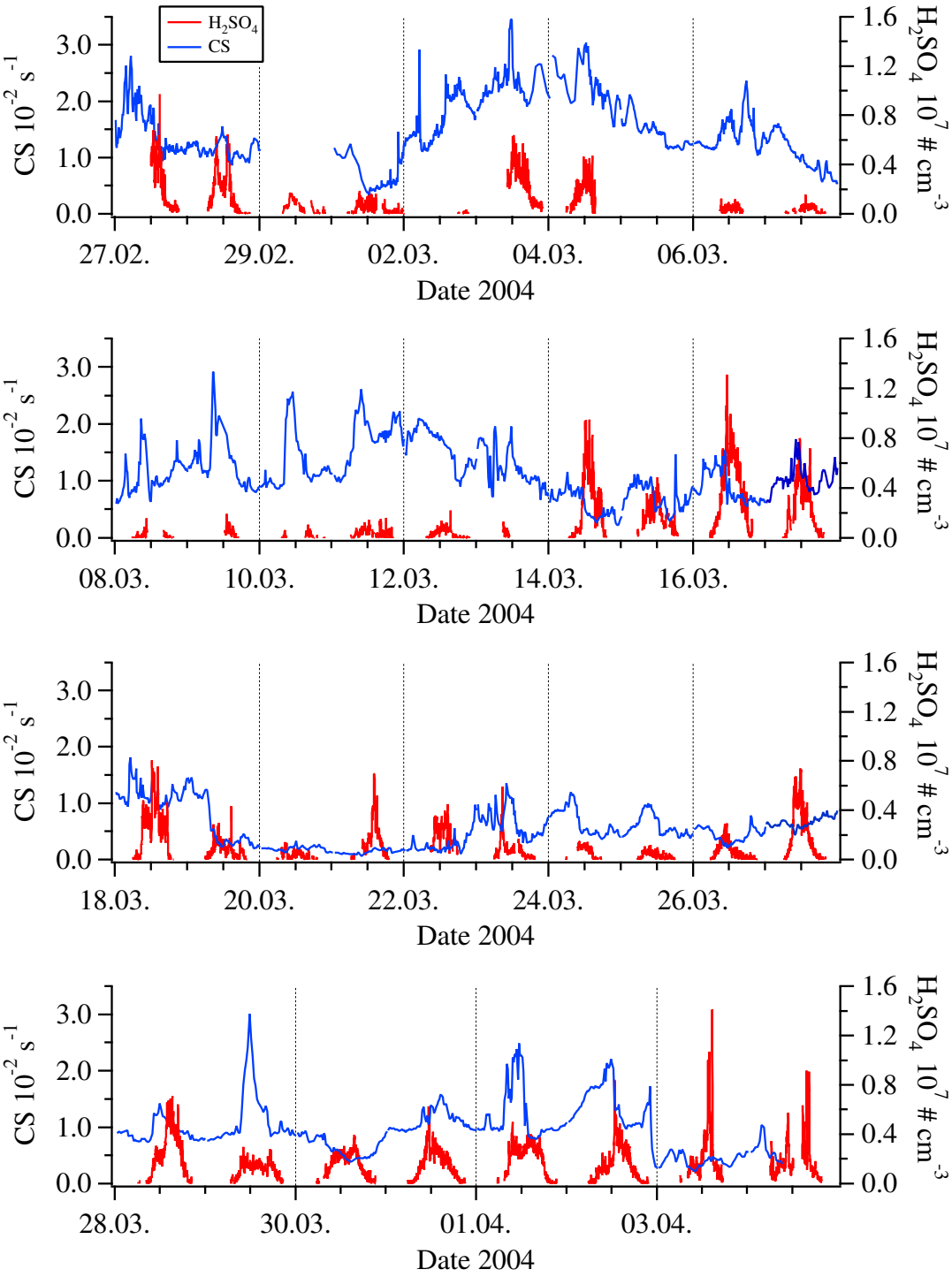

Figure 7.4: Heidelberg: H_2SO_4-concentrations (red line) and Condensation Sink (blue line) versus Time. (Note: different y-axis scale for CS compared to Figure 7.3)

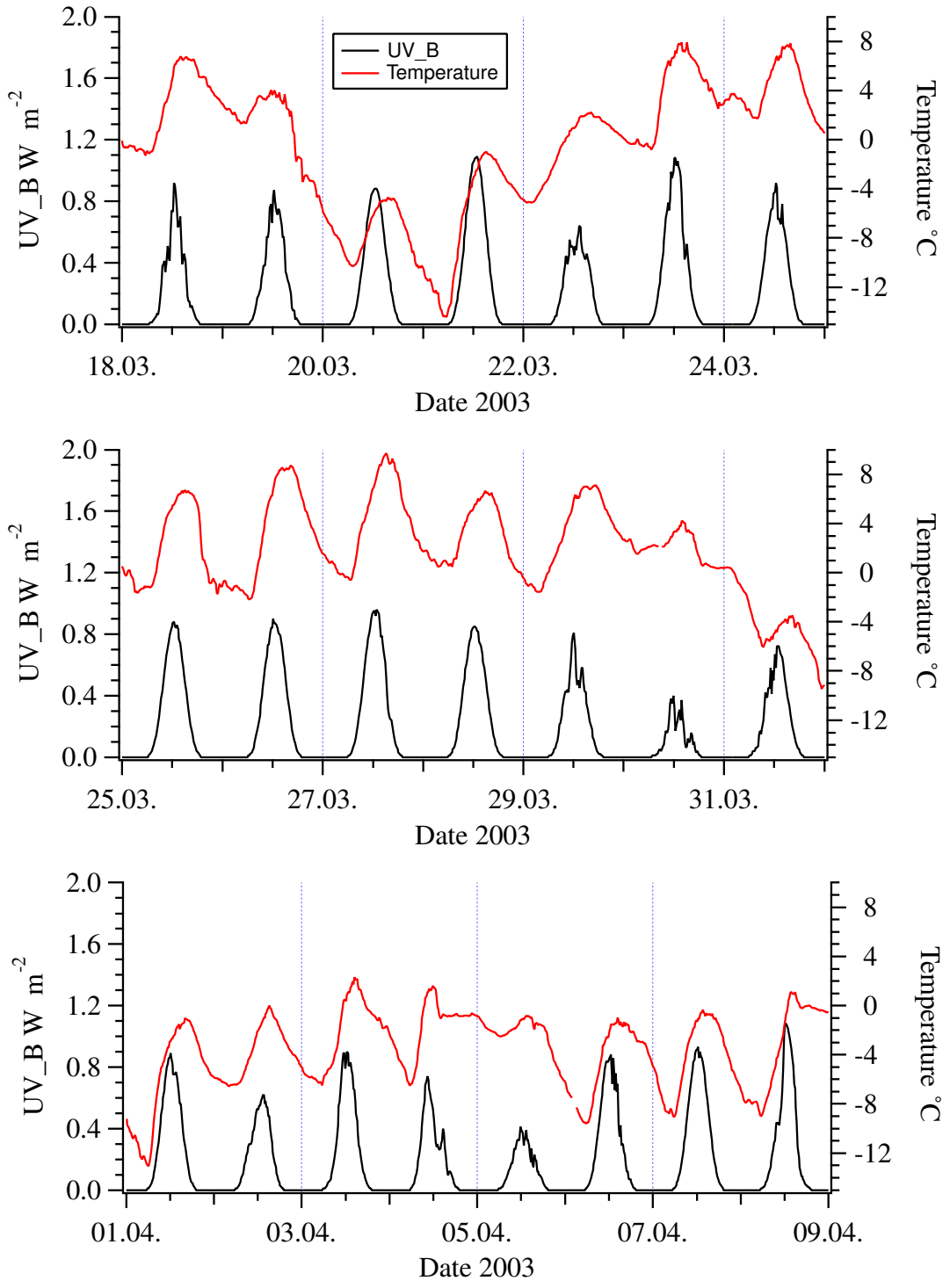

Figure 7.5: Hyytiälä: UV-B radiation (black line) and temperature (red line) versus time.

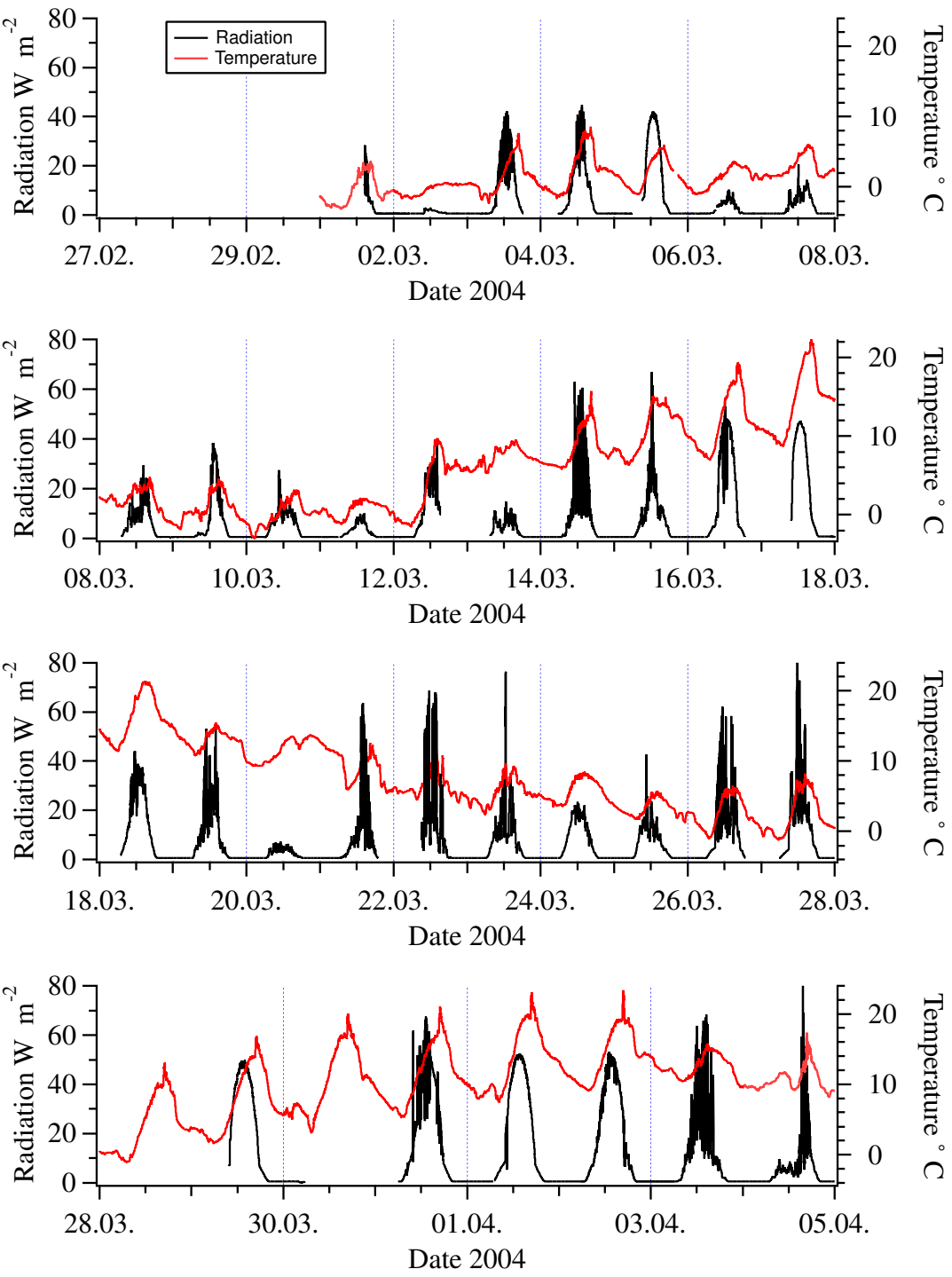

Figure 7.6: Heidelberg: Total radiation (black line) and temperature (red line) versus time.

During QUEST 2 almost all days were sunny whereas the days during QUEST 3b were often cloudy or rainy especially in the beginning of March. On those days very low values of sulphuric acid were measured. The mean temperature was about 10°C in Heidelberg and about 2°C in Hyytiälä.

Chapter 8

Results and Discussion

In this chapter all *calculated* values will be presented and the results of the comparison between the two measurement sites Hyytiälä and Heidelberg will be discussed.

Table 8.1 gives an overview of all values on event days calculated directly from DMPS plots and **Table 8.2** gives the same calculated parameters taking GR2 as input values. Overall the mean values for all calculated quantities were higher in Heidelberg compared to Hyytiälä. For most values like CS and H_2SO_4 we would expect this due to the higher polluted air in Heidelberg.

8.1 Growth Rates and Nucleation Rates

The growth rate GR1 ranges from 1.7 to 12.2 nm h^{-1} in Hyytiälä and from 2.1 to 22.9 nm h^{-1} in Heidelberg with a mean of 4.2 and 9.1 nm h^{-1}, respectively. Furthermore the growth rate in Heidelberg showed a stronger variability. From the timeshift calculations we obtained on each day a smaller growth rate for the Hyytiälä data with a mean value of 1.1 nm h^{-1} (**Table 8.2**). This is consistent with the result by Kulmala [Kulmala et al., 2004a], who found that the growth is always smaller for the first nanometers of growth than for later growth. An explanation could be that larger particles grow possibly faster due to a condensable trace gas x which cannot condense on small particles (Kelvin-effect). For the Heidelberg data this relation could not be seen and GR2 (mean 8.99 nm h^{-1}) was often higher than GR1 (mean of 8.3 nm h^{-1}).

Date	Start	Class	GR 1	J	C_{vap}	H_2SO_4	CS mean	Q	Perc. H_2SO_4
			nm h^{-1}	$cm^{-3}s^{-1}$	10^8 cm^{-3}	10^6 cm^{-3}	$10^{-3}s^{-1}$	10^5 $cm^{-3}s^{-1}$	%
Hyytiälä									
18.03.2003	12:00	2	1,6	0,27	0,22	2,1	1,0	0,22	9,5
19.03.2003	12:00	3	3,0	0,23	0,41	0,6	0,9	0,37	1,5
20.03.2003	10:00	1	1,7	0,46	0,23	2,2	0,8	0,18	9,6
21.03.2003	10:00	1	3,1	1,11	0,42	3,7	1,9	0,80	8,8
23.03.2003	10:00	3	4,2	0,28	0,58	2,0	3,0	1,74	3,4
24.03.2003	10:00	2	3,1	0,32	0,42	1,4	0,6	0,25	3,3
25.03.2003	10:00	1	2,6	0,49	0,36	2,6	1,1	0,40	7,2
26.03.2003	10:00	2	3,9	1,00	0,53	4,4	2,9	1,54	8,3
27.03.2003	13:30	3	3,0	0,10	0,41	3,4	4,1	1,68	8,3
28.03.2003	10:00	1	3,3	0,45	0,45	1,8	1,7	0,77	4,0
29.03.2003	10:30	2	6,0	1,72	0,82	2,3	2,3	1,89	2,8
31.03.2003	13:00	3	4,1	1,01	0,56	2,6	1,0	0,56	4,6
01.04.2003	10:00	1	2,3	2,13	0,32	3,2	1,8	0,58	10,0
02.04.2003	10:00	1	5,1	1,22	0,70	3,8	3,3	2,31	5,4
03.04.2003	10:00	2	12,2	2,45	1,67	7,6	3,6	6,01	4,6
04.04.2003	10:00	1	4,9	6,97	0,67	3,2	1,4	0,94	4,8
06.04.2003	09:00	3	1,8	0,14	0,25	1,7	0,8	0,20	6,8
07.04.2003	08:00	2	9,0	1,12	1,23	5,3	1,2	1,48	4,3
08.04.2003	09:00	1	6,2	1,16	0,85	3,9	1,9	1,62	4,6
mean			4,27	1,20	0,58	3,0	1,9	1,24	5,9
Heidelberg									
14.03.2004	12:00	1	14,20	2,42	1,95	2,7	4,08	7,96	1,4
15.03.2004	12:00	3	22,90	3,82	3,14	2,6	5,14	16,14	0,8
16.03.2004	12:00	1	5,70	1,30	0,78	6,3	7,14	5,57	8,1
18.03.2004	12:00	2	8,10	5,95	1,11	4,4	11,27	12,51	4,0
21.03.2004	12:00	2	7,80	0,65	1,07	2,4	1,64	1,75	2,2
22.03.2004	10:00	2	2,10	0,65	0,29	2,4	1,88	0,55	8,3
28.03.2004	14:00	3	6,70	1,42	0,92	4,2	9,68	8,91	4,6
30.03.2004	14:00	1	13,39	3,33	1,84	2,2	4,28	7,88	1,2
02.04.2004	12:00	3	3,30	4,63	0,45	3,2	11,63	5,23	7,1
03.04.2004	12:00	3	5,70	2,50	0,78	4,2	4,14	3,23	5,4
mean			8,99	2,67	1,23	3,5	6,09	6,97	4,3

Table 8.1: All calculated values starting from growth rate 1: Nucleation rate J, condensable vapor C_{vap}, mean H_2SO_4-concentration, mean condensation sink CS, source rate Q, H_2SO_4-percentage of the condensable vapor.

Date	GR 2	C_{vap}	H_2SO_4	CS mean	Q	Perc. H_2SO_4
	nm h^{-1}	10^8 cm^{-3}	10^6 cm^{-3}	10^{-3} s^{-1}	10^5 cm^{-3} s^{-1}	%
Hyytiälä						
18.03.2003	0,7	0,10	2,0	1,0	0,10	20,1
19.03.2003	0,5	0,07	1,0	0,9	0,06	6,8
20.03.2003	0,7	0,10	1,0	0,8	0,08	10,0
21.03.2003	1,1	0,16	4,0	1,9	0,30	25,6
23.03.2003	0,7	0,09	1,0	3,0	0,27	11,0
24.03.2003	-	-	-	0,6	-	-
25.03.2003	1,3	0,18	1,0	1,1	0,20	5,5
26.03.2003	1,0	0,14	1,0	2,9	0,41	7,3
27.03.2003	2,0	0,27	3,0	4,1	1,11	11,0
28.03.2003	1,0	0,14	2,0	1,7	0,24	14,6
29.03.2003	1,3	0,18	2,0	2,3	0,41	11,0
31.03.2003	0,6	0,08	1,0	1,0	0,08	11,9
01.04.2003	1,3	0,18	2,0	1,8	0,32	11,0
02.04.2003	0,4	0,06	2,0	3,3	0,20	34,7
03.04.2003	4,0	0,55	1,0	3,6	1,98	18,3
04.04.2003	0,8	0,11	2,0	1,4	0,15	18,3
06.04.2003	1,3	0,18	1,0	0,8	0,14	5,5
07.04.2003	1,3	0,18	1,0	1,2	0,22	5,5
08.04.2003	1,0	0,14	1,0	1,9	0,27	7,3
mean	1,1	0,16	1,6	1,86	0,34	13,1
Heidelberg						
14.03.2004	8,0	1,1	3,0	4,08	4,5	2,7
15.03.2004	4,0	0,5	2,0	5,14	2,6	4,0
16.03.2004	8,0	1,1	5,0	7,14	7,9	4,6
18.03.2004	8,0	1,1	6,0	11,27	12,4	5,5
21.03.2004	8,0	1,1	2,0	1,64	1,8	1,8
22.03.2004	4,0	0,5	2,0	1,88	0,9	4,0
28.03.2004	8,0	1,1	3,0	9,68	10,6	2,7
30.03.2004	13,3	1,8	3,0	4,28	7,7	1,7
02.04.2004	13,3	1,8	2,0	11,63	20,9	1,1
03.04.2004	8,0	1,1	4,0	4,14	4,6	3,6
mean	8,3	1,1	3,2	6,09	7,4	3,2

Table 8.2: Calculated values starting from growth rate 2: Condensable vapor C_{vap}, mean H_2SO_4-concentration during timeshift interval, mean condensation sink CS, source rate Q, H_2SO_4-percentage of the condensable vapor. (No H_2SO_4-concentration measurements in the morning on 24.03.2003)

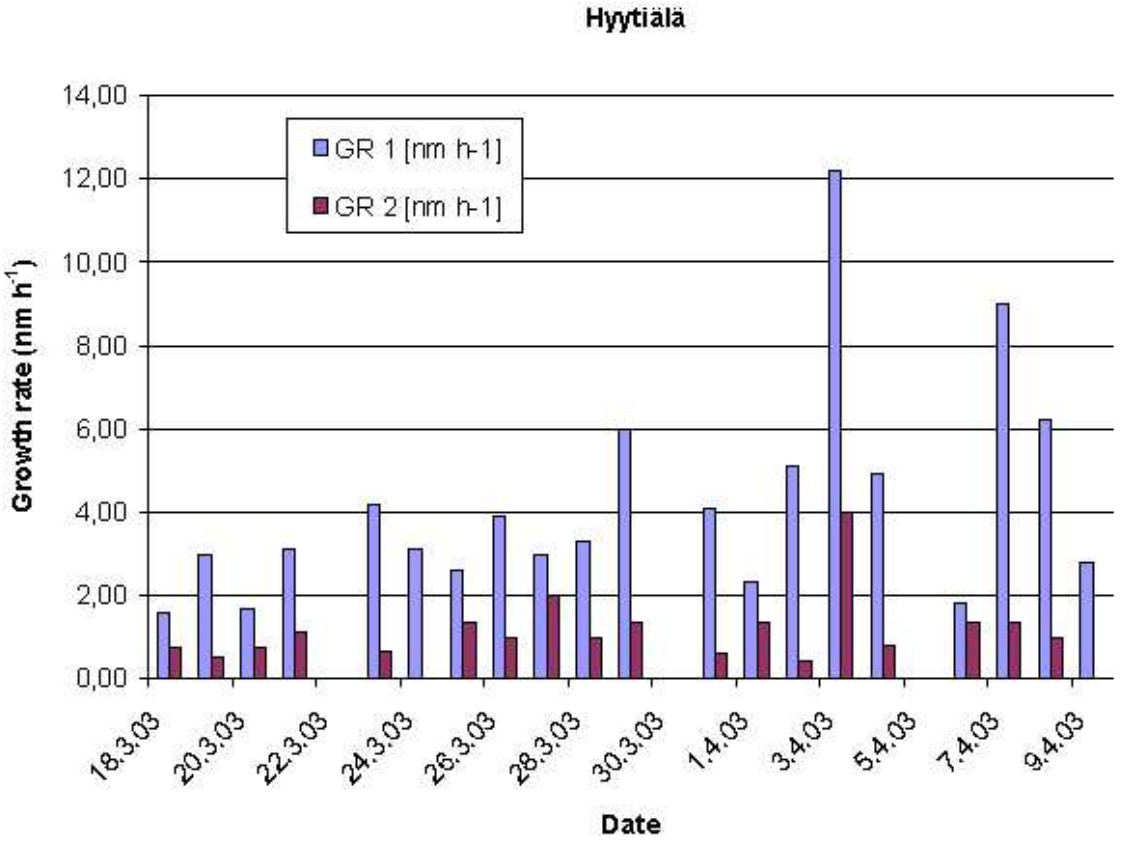

Figure 8.1: Growth rate 1 and growth rate 2 for days with aerosol particle events in Hyytiälä.

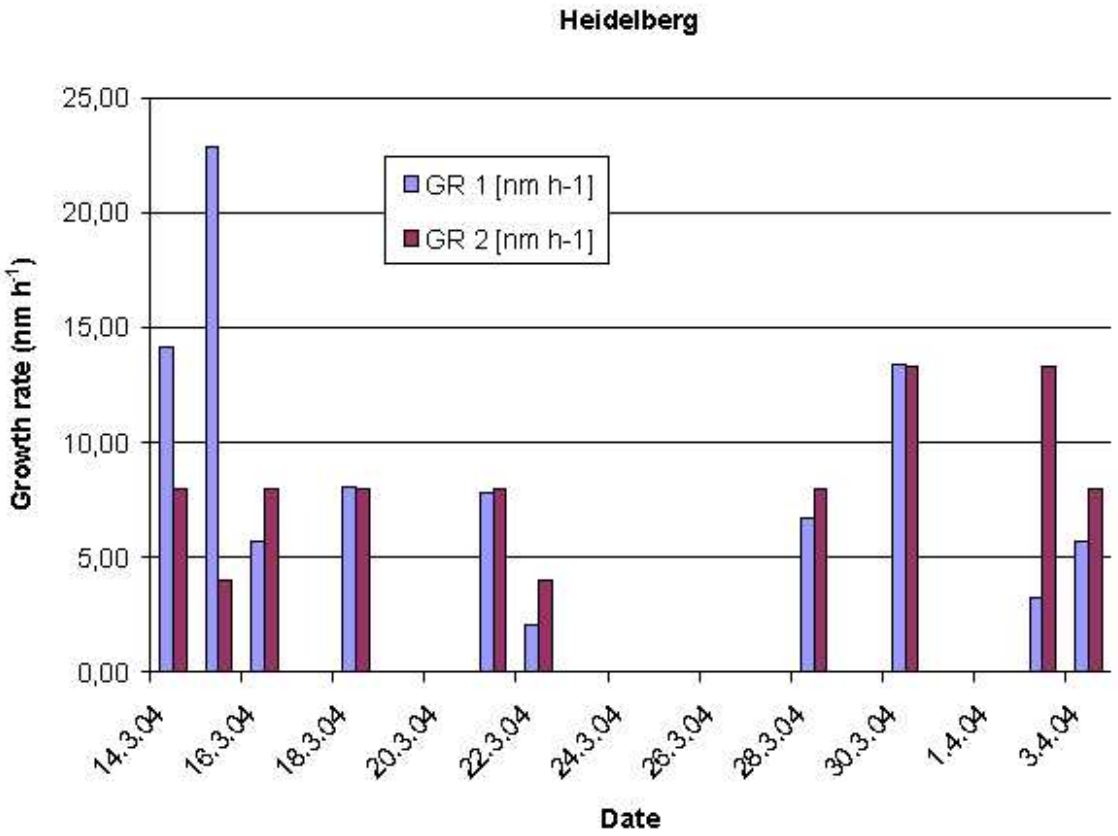

Figure 8.2: Growth rate 1 and growth rate 2 for days with aerosol particle events in Heidelberg.

Figures 8.1 and 8.2 show both growth rates for Hyytiälä and Heidelberg, respectively. Possible reasons for the nearly equal growth rates GR1 and GR2 in Heidelberg could be that the condensable trace gases, here especially ones with very low saturation vapor pressures, are probably different in regions influenced mainly by anthropogenic pollution sources to regions with mainly natural sources. So it might be that organic compounds of urban origin condense easier on one nanometer aerosol particles than the natural ones and that consequently those different gases cause different growth rates in the beginning (GR2). A second reason could be that in Heidelberg local sources with high amounts of small particles increase the preexistent aerosol particle concentration. In these cases the used timeshift analysis is inadequate and will overestimate growth rate GR2.

The nucleation rates J were quite similar in Hyytiälä and Heidelberg with mean values of 1.2 and 2.7 cm^{-3} s^{-1} and they were usually highest on class 1 event days. The result that the highest formation rates in Hyytiälä are visible on clear event days is in agreement with results previously published by [Boy et al., 2003]. With a low background particle concentration, a high amount of the condensable vapor is available for new particle formation.

8.2 Condensable Vapor and Source Rates

From the growth rates the condensable vapor concentration C_{vap} was determined according to section 7.1.4. Afterwards C_{vap} was compared to the measured sulphuric acid concentration in order to quantify the contribution of sulphuric acid to the formation and growth rates. In case of GR1, the mean value of the sulphuric acid concentration during a time interval beginning with the starting time of the formation event and ending in the evening was used. In case of GR2, a different H_2SO_4-concentration was used because the timeshift analysis is just applied on the first rise of the H_2SO_4-curve, as explained above. Consequently, the mean sulphuric acid concentration during the timeshift interval was used.

C_{vap} and the percentage of sulphuric acid to the growth rates were determined for GR1 and GR2. The results are compiled in **Tables 8.1 and 8.2**. The percentage contribution of sulphuric acid to the particle growth in Hyytiälä was higher for GR2 (mean 13.1 %) than for GR1 (mean 5.9 %). So it seems that in Hyytiälä sulphuric acid plays a bigger role in formation

and the first nanometers of growth than in later growth. In Heidelberg this behavior could not be seen, moreover both percentages were about the same (mean 4.3 % for GR1 and 3.2 % for GR2). Here again high concentrations of urban organic acids could be responsible. They might partly substitute sulphuric acid in its important role specifically in aerosol formation and initial growth.

Furthermore, the percentage contribution calculated from GR1 was almost the same at both measurement sites (5.9 and 4.3 %), which means that sulphuric acid seems to contribute to later particle growth always in about the same percentage, independent from the region.

Subsequently the source rate Q was calculated from the condensable vapor concentration and the mean condensation sink according to equation (7.5). Q depends only on these two parameters and consequently it was higher in Heidelberg than in Hyytiälä. Again the more polluted air in Heidelberg should be the reason for the higher source rates of sulphuric acid.

8.3 Correlations

The next point analyzed was the correlation between sulphuric acid and the smallest detectable particles between 3 and 6 nm (N3). As mentioned above we would expect a similar shape of the two curves H_2SO_4 versus time and N3 versus time with a certain time lag due to the fact that sulphuric acid is one important factor involved in new particle formation. More precisely, if sulphuric acid was the only substance responsible for new particle formation, both curves should have exactly the same shape. Consequently, the correlation between those two curves indicates the relation between sulphuric acid and newly formed aerosols.

Figures 8.3 and 8.4 give one example of these analyses for Hyytiälä and Heidelberg, respectively. In these figures N3 is plotted versus H_2SO_4. There were good correlations on some days like the examples shown but there were also days where no correlation was found; especially for the data in Heidelberg the correlation was much worse than expected on many days. **Figure 8.5** presents the correlation on all event days firstly for Hyytiälä, secondly for Heidelberg and thirdly for both sites. Both scatter plots show a similar pattern. Three items are remarkable: There seems to be an upper threshold for the number of particles that are formed by a certain amount of H_2SO_4. Secondly, in Hyytiälä even with high amounts

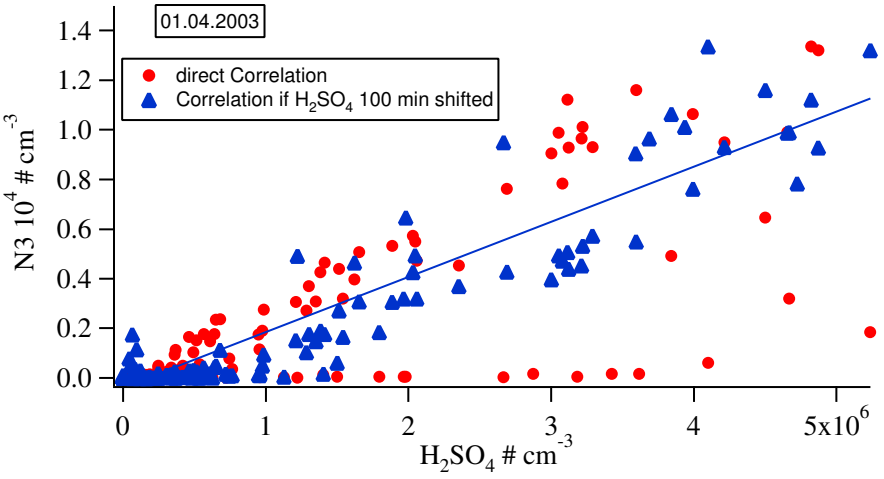

Figure 8.3: Scatter plot of N3 and H_2SO_4 for one day (1st April 2003) in Hyytiälä. "Direct correlation" means that no time lag was taken into consideration, "Correlation after 100 min" means that a time lag of 100 min was considered.

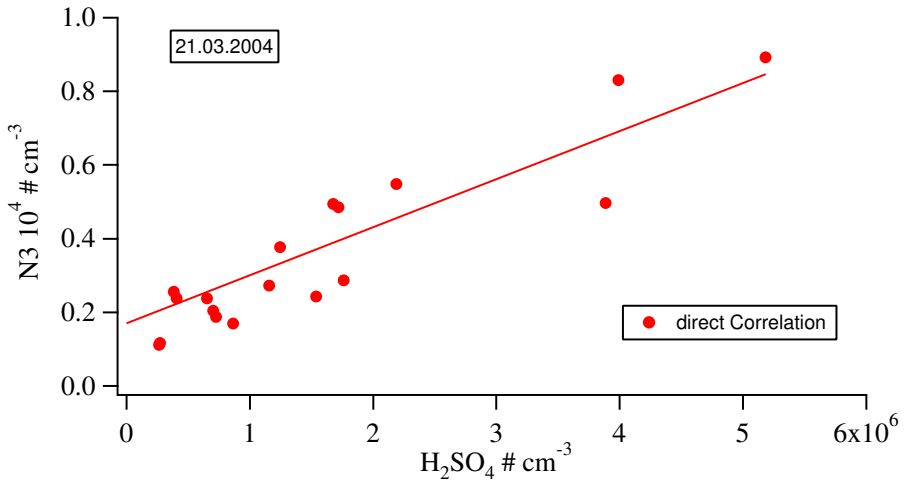

Figure 8.4: Scatter plot of N3 and H_2SO_4 for one day (21st March 2004) in Heidelberg.

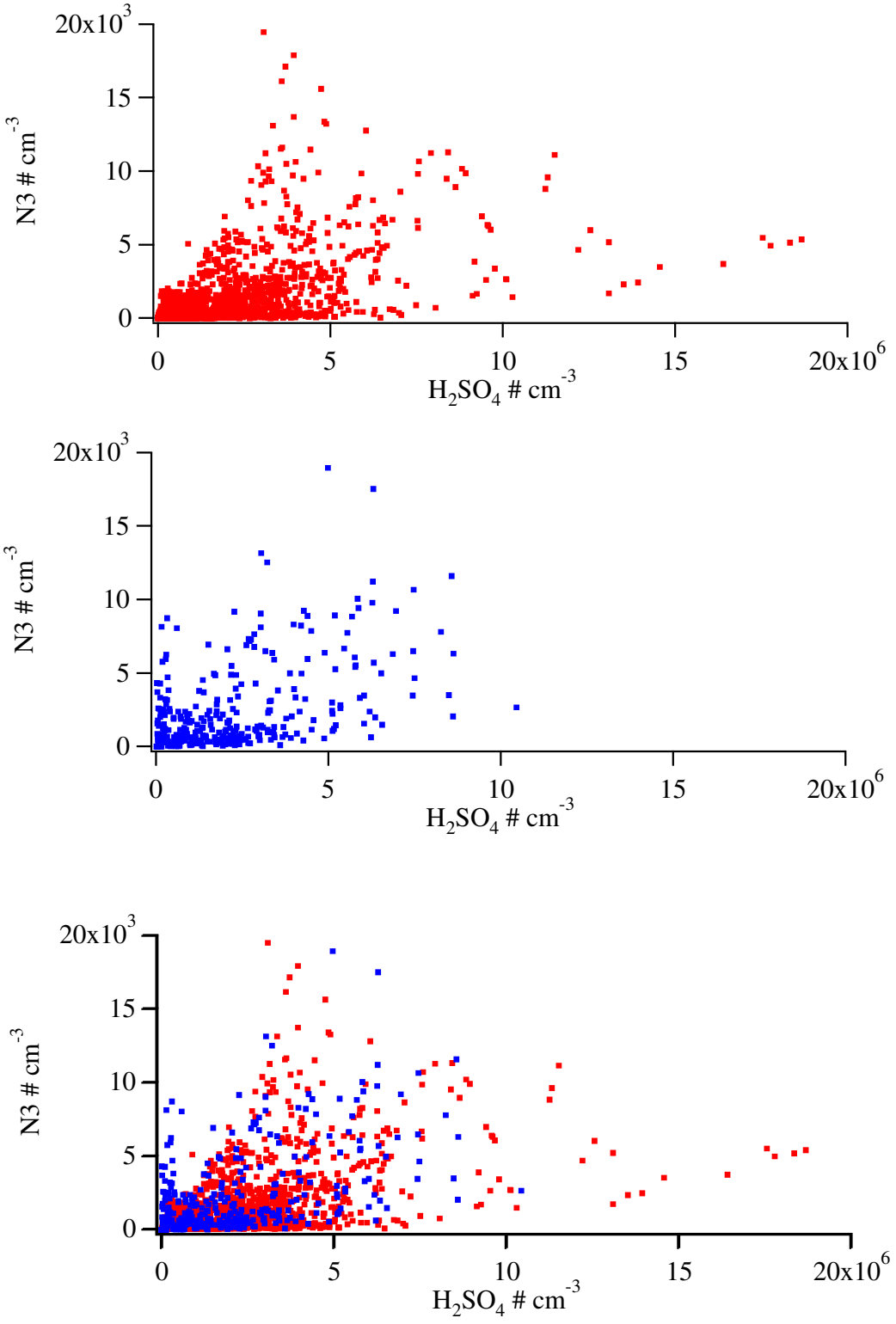

Figure 8.5: Correlation for all days: Top panel Hyytiälä, middle panel Heidelberg, bottom panel both sites.

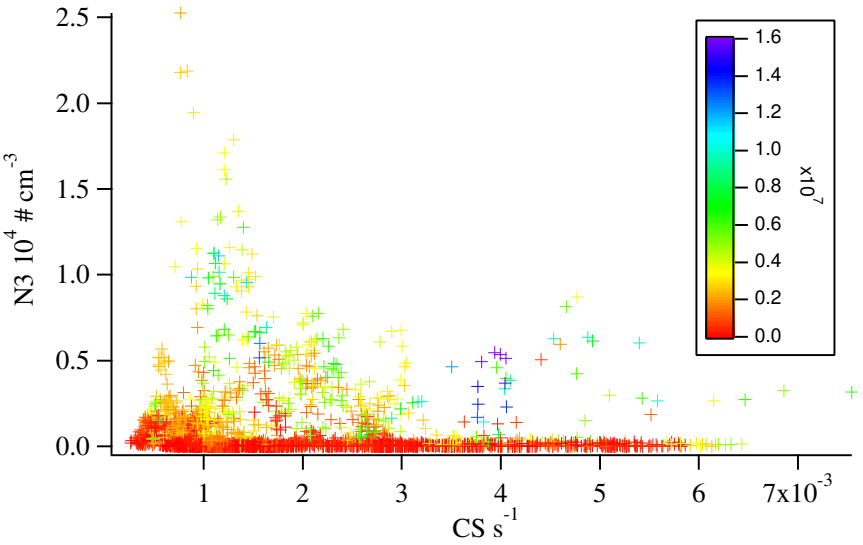

Figure 8.6: N3 plotted versus the condensation sink (Hyytiälä), the H_2SO_4-concentration is given as color code.

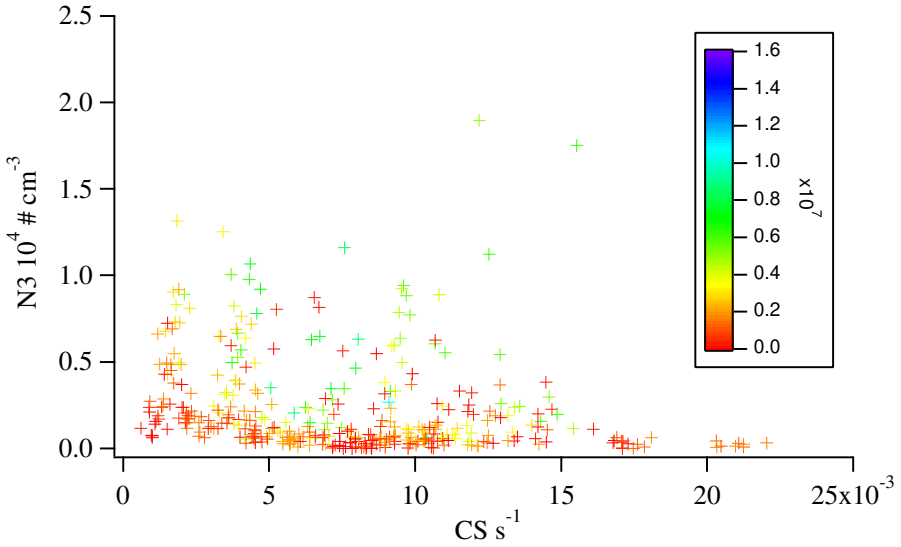

Figure 8.7: N3 plotted versus the condensation sink (Heidelberg), the H_2SO_4-concentration is given as color code. Note: x-axis scale differs from Figure 8.6.

of H_2SO_4 (15 - $20{\cdot}10^6$) only a small amount of N3 is formed ($5 \cdot 10^3$), which means that another sink than particle formation exists for H_2SO_4 in Hyytiälä. Thirdly, in Heidelberg even without a significant H_2SO_4-concentration high numbers of small particles exist. This could be explained by local pollution or other condensable vapors that substitute sulphuric acid in aerosol formation.

If we compare **Figure 8.6 and Figure 8.7**, which show the particle number concentration between 3 and 6 nm plotted versus the condensation sink at both measurement sites and the sulphuric acid concentration as color code, we recognize that in Hyytiälä the concentration of small particles is highest at low CS values and decreases steeply for high CS values. Or with high CS values at least high concentrations of sulphuric acid are needed in order to get a significant amount of small new particles. Yet in Heidelberg high N3 values occur even with high CS and low sulphuric acid values. This could be explained once more by local and temporarily high emission of particles and/or high amounts of condensable vapors by anthropogenic sources. During these periods sulphuric acid may contribute only partly to the formation of the N3 aerosols, which would explain the bad correlations.

8.4 Air Mass Trajectories

Finally air trajectories (5 days backward trajectories) on event days were investigated. For Hyytiälä data it has already been shown that on event days with less polluted air, originating over polar or atlantic regions, CS is 2.64 times, sulphuric acid 1.46 times and growth rates are 1.45 times lower than on days with polluted air masses originating over industrial areas [Boy et al., 2004]. In Heidelberg it was practically impossible to get days with clear, non polluted air because of its central European site. Nevertheless, events were preferably found on days with air masses from southwest directions, originating over the Mediterranean sea or southern atlantic, whereas no events occurred mainly on days with air masses originating over the North sea or Baltic sea, which approach Heidelberg from the North and North-West (see **Table 8.4**).

		Hyytiälä	Heidelberg
CS	$[10^{-3}\ s^{-1}]$	2,90	6,09
H_2SO_4	$[10^{6}\ cm^{-3}]$	3,31	3,50
GR	$[nm\ h^{-1}]$	3,20	8,99

Table 8.3: Comparison of condensation sink, H_2SO_4-concentration and growth rate for Hyytiälä and Heidelberg on polluted days.

Table 8.3 compiles mean values of condensation sink, sulphuric acid concentration and growth rate on *polluted* days in Finland and Germany. The mean values for Hyytiälä are taken from [Boy et al., 2004]. CS and GR are 2 to 3 times higher in Heidelberg compared to Hyytiälä; a fact which was pointed out already earlier and reflects the higher anthropogenic pollution influence in Central Europe compared to Northern Europe. Since the H_2SO_4-concentrations are quite similar at both sites, we come a third time to the conclusion that other vapors than sulphuric acid seem to play a very important role in particle formation.

Events	Trajectory	Direction	Frequency
14.03.	Balearic Islands, Southern France	SW	SW=3
15.03.	Sardinia, Southern France	SW	W=2
16.03.	Croatia, Northern Italy	SE	NE=2
18.03.	Atlantic, France, Switzerland	SW	SE=1
21.03.	Atlantic, France	W	
22.03.	Atlantic, France	W	
28.03.	Sweden, Baltic sea	NE	
30.03.	Southern Finland, Baltic sea	NE	
No Events			
25.02.	Greenland, North Sea	N	N=7
26.02.	Greenland, North Sea	N	NW=6
27.02.	Iceland, GB, Belgium	NW	W=5
28.02.	GB, Belgium, North Sea	NW	SW=3
01.03.	GB, Belgium, Eastern Germany	NE	NE=3
02.03.	North Sea, Turn over Germany	N	SE=2
03.03.	Eastern Germany, Netherlands, Belgium	NW	E=1
04.03.	Eastern Germany, Denmark, Belgium	N	
05.03.	Eastern Germany, Netherlands, Belgium	NW	
06.03.	Northern Germany, Alsace, Switzerland	SW	
07.03.	Belgium, Alsace	W	
08.03.	Belgium	W	
09.03.	Baltic Sea, Eastern Germany, Netherlands	NW	
10.03.	Baltic Sea, Northern Germany	N	
11.03.	Eastern Germany, Czech Rep.	E	
12.03.	Germany, Czech Rep., Croatia, Italy, Switzerland	SE	
13.03.	Sweden, Heidelberg, Southern France	SW	
17.03.	First Croatia, Italy, 12 utc suddenly Atlantic, France	W	
19.03.	Balearic Islands, Southern France	SW	
20.03.	Galicia, Atlantic, France	W	
23.03.	Atlantic, France	W	
24.03.	Atlantic, GB, Netherlands	NW	
25.03.	Shetland, North Sea	N	
26.03.	Shetland, Denmark	N	
27.03.	Russia, Finland, Sweden, Eastern Germany	NE	
29.03.	Sweden, Eastern Germany, Bavaria	NE	
31.03.	Belarus, Poland, Northern Italy	SE	

Table 8.4: Air mass trajectories (Heidelberg). On each day the trajectory was given for the 5 previous days. In the column "Frequency" is compiled how often a wind direction occurred.

Chapter 9

Conclusions and Perspectives

In this work measurements of atmospheric gaseous sulphuric acid have been carried out during the European project QUEST. The measurement method (CIMS = chemical ionization mass spectrometry) has been described and the measured data have been presented. Afterwards these measurements have been compared to gaseous sulphuric acid measurements carried out by our group previously in Hyytiälä, Finland, during QUEST 2. Both gaseous H_2SO_4 data sets were discussed in the light of simultaneously measured aerosol data.

First of all higher measured condensation sink and growth rate values were found in Heidelberg compared to Hyytiälä which can be explained by the more severely polluted air in Heidelberg. Nevertheless, the measured gaseous sulphuric acid concentrations were about the same at both measurement sites. This also concerns the percentage contribution of sulphuric acid to new particle formation and growth at both sites (5.9 and 4.3 % respectively) in case of growth rate GR1 (a total growth rate for the whole event) which could mean that sulphuric acid contributes to particle growth always in about the same percentage, independent from the region. Growth rate GR2, calculated with the newly developed timeshift analysis, gave a growth rate especially for the initial growth from 1 nm up to a size of 3 nm. The values were in average smaller than GR1 in Hyytiälä, which was already earlier pointed out by Kulmala, so the growth seems to be initially slower compared to later. Moreover, the percentage contribution of sulphuric acid to particle growth was higher in Hyytiälä in the beginning (13.1 % for GR2 and 5.9 % for GR1), which means that sulphuric acid seems to have a bigger role in the first two nanometers of growth than in later growth.

Contrarily, in Heidelberg both growth rates were about the same. This may be explained by the influence of other gaseous condensable substances, especially compounds with low saturation vapor pressure and anthropogenic origin, that might substitute H_2SO_4 in its important role in new particle formation and growth. Moreover, the timeshift analysis gives inadequate results if the correlation between H_2SO_4 and N3 is not very pronounced. A correlation analysis between sulphuric acid and the particles between 3 and 6 nm gave exactly this result, i.e. the correlation in Hyytiälä was quite clear in contrast to Heidelberg. Generally the results in Heidelberg were less clear; most probable temporarily and locally high amounts of other low saturation vapor pressure compounds from anthropogenic sources mask the influence of sulphuric acid.

In future experiments it would be desirable to find out the nature of those other substances. In recent years it has already been speculated that certain volatile organic compounds (VOC) may be responsible. However, the analysis of VOC's is quite difficult because of the wide range of substances, often different substances with the same molecular mass. The measurement instrument IT-CIMS with its possibility to realize fragmentation analyses could lead to more detailed results at this point. A fourth part of the QUEST project is planned, probably again in Finland. In the framework of this project a search for condensable VOC's should be carried out.

Appendix A

Site Maps

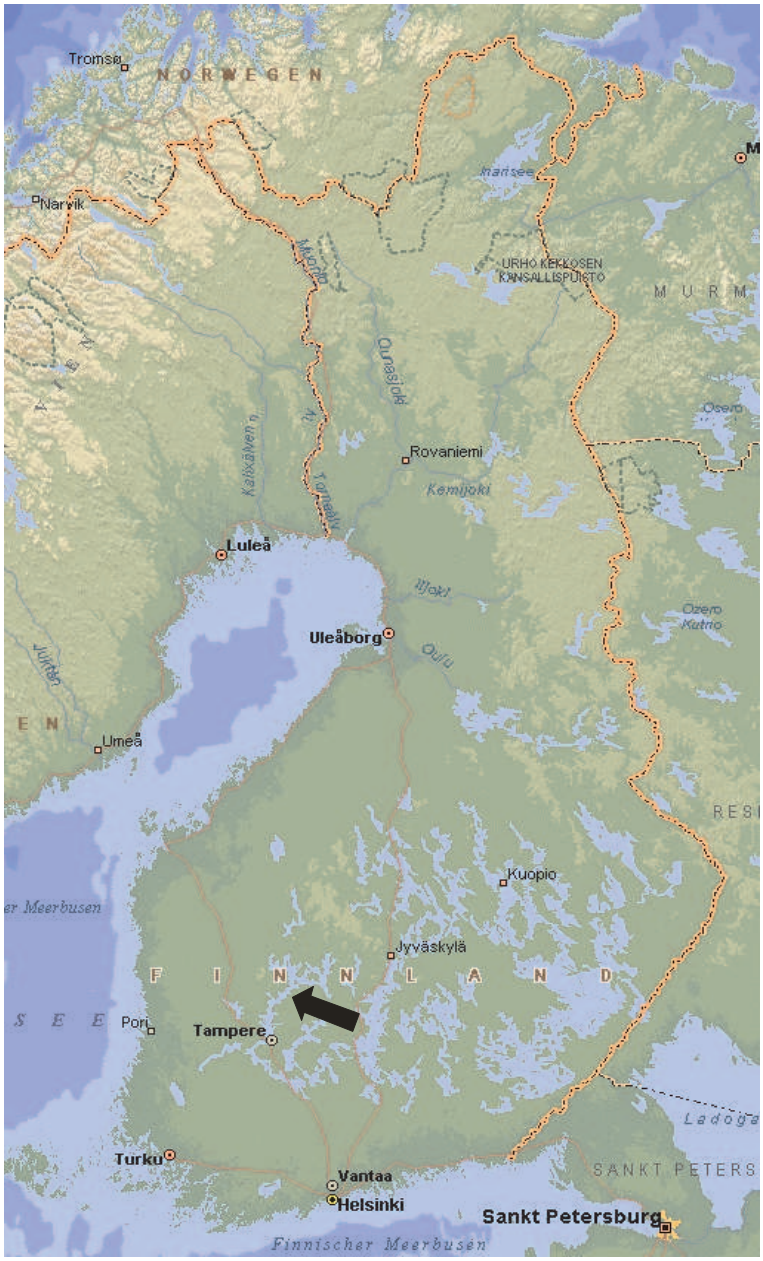

Figure A.1: Map of Finland. The black arrow indicates the measurement site Hyytiälä ($61°51'N, 24°17'E, 181\ m\ asl$). The main wind direction is west-south-west, so direction from Tampere city.

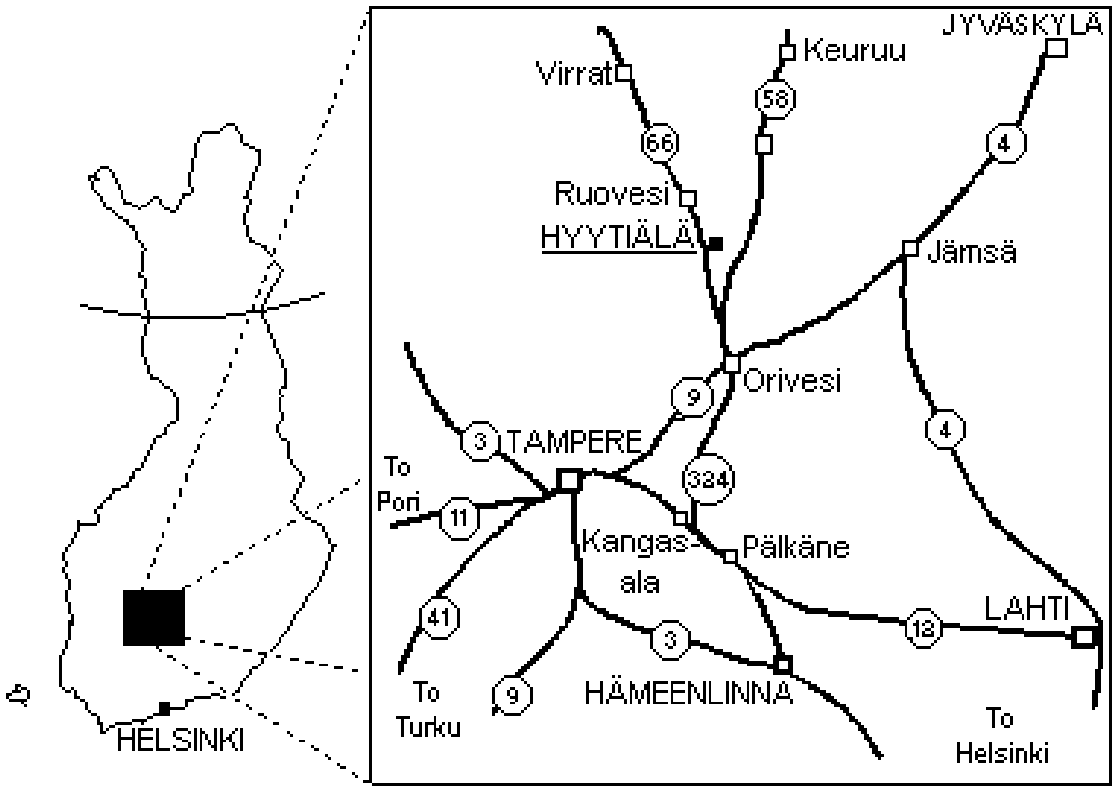

Figure A.2: Map of Hyytiälä.

Figure A.3: Map of Germany. The black arrow indicates the measurement site Heidelberg ($49°23'N, 08°41'E, 350\ m\ asl$) and here the arrow also gives the favorite wind direction west-south-west.

Figure A.4: Map of Heidelberg. The MPI-K is marked with a red ellipse.

Appendix B

PITMAS-HEADER and typical Spectra

This HEADER was taken on the 30th of March around noon. All indicated values are a typical example for the usual values applied during operation.

	SCAN
344	Scan Number
2	Number of Packets
356,131	Start Time
50,00	Low Mass
300,00	High Mass
943328,00	TIC
125,00	Base Peak Mass
173433,00	Base Peak Intensity
0	Number of Channels
0,000	Sampling Rate
Off	Wideband Activation
10	Micro Scan Count
5715.28	Ion Injection Time (ms)
0	Scan Segment
0	Scan Event
58.55	Elapsed Scan Time (sec)
0.00	API Source CID Energy
N/A	Resolution
No	Average Scan by Inst
No	BackGd Subtracted by Inst
0	Charge State

	API SOURCE (**Not in use**)
4.49	Source Voltage (kV)
0.29	Source Current (uA)
No	Vaporizer Thermocouple OK
-0.00	Vaporizer Temp (C)
60.20	Sheath Gas Flow Rate ()
0.11	Aux Gas Flow Rate()
No	Capillary RTD OK
0.51	Capillary Voltage (V)
514.60	Capillary Temp (C)
-50.00	Tube Lens Voltage (V, set point)
No	8 kV supply at limit
	VACUUM
Yes	Vacuum OK
Yes	Ion Gauge Pressure OK
On	Ion Gauge Status
2.28	Ion Gauge (x10e-5 Torr)
Yes	Convectron Pressure OK
4.99	Convectron Gauge (Torr)
	TURBO PUMP
Running	Status
35677	Life (hours)
60000	Speed (rpm)
56	Power (Watts)
40.00	Temperature (C)
	ION OPTICS
Yes	Multipole Frequency On
3.80	Multipole 1 Offset (V)
6.67	Lens Voltage (V)
12.44	Multipole 2 Offset (V)
960.00	Multipole RF Amplitude (Vp-p, set point)
9.88	Coarse Trap DC Offset (V)
	MAIN RF
Yes	Reference Sine Wave OK
Yes	Standing Wave Ratio OK
63.00	Main RF DAC (steps)
-0.00	Main RF Detected (V)
35.06	RF Detector Temp (C)
0.03	Main RF Modulation (V)
8.97	Main RF Amplifier (Vp-p)
29.15	RF Generator Temp (C)
	ION DETECTION SYSTEM
-1062.57	Multiplier Actual (V)

	POWER SUPPLIES
5.08	+5V Supply Voltage (V)
-14.94	-15V Supply Voltage (V)
14.91	+15V Supply Voltage (V)
23.75	+24V Supply Voltage (V)
-28.07	-28V Supply Voltage (V)
28.27	+28V Supply Voltage (V)
0.85	+28V Supply Current (Amps)
32.58	+35V Supply Voltage (V)
35.85	+36V Supply Voltage (V)
-145.35	-150V Supply Voltage (V)
147.23	+150V Supply Voltage (V)
-197.09	-205V Supply Voltage (V)
203.86	+205V Supply Voltage (V)
29.69	Ambient Temp (C)
	INSTRUMENT STATUS
On	Instrument
Acquiring	Analysis
	SYRINGE PUMP (**Not in use**)
Ready	Status
3.00	Flow Rate (uL/min)
0.00	Infused Volume (uL)
2.30	Syringe Diameter (mm)
	DIGITAL INPUTS
No	READY IN is active
No	START IN is active
Error	Divert/Inject valve

Table B.1: Example for a PITMAS-HEADER, all usual values are indicated here.

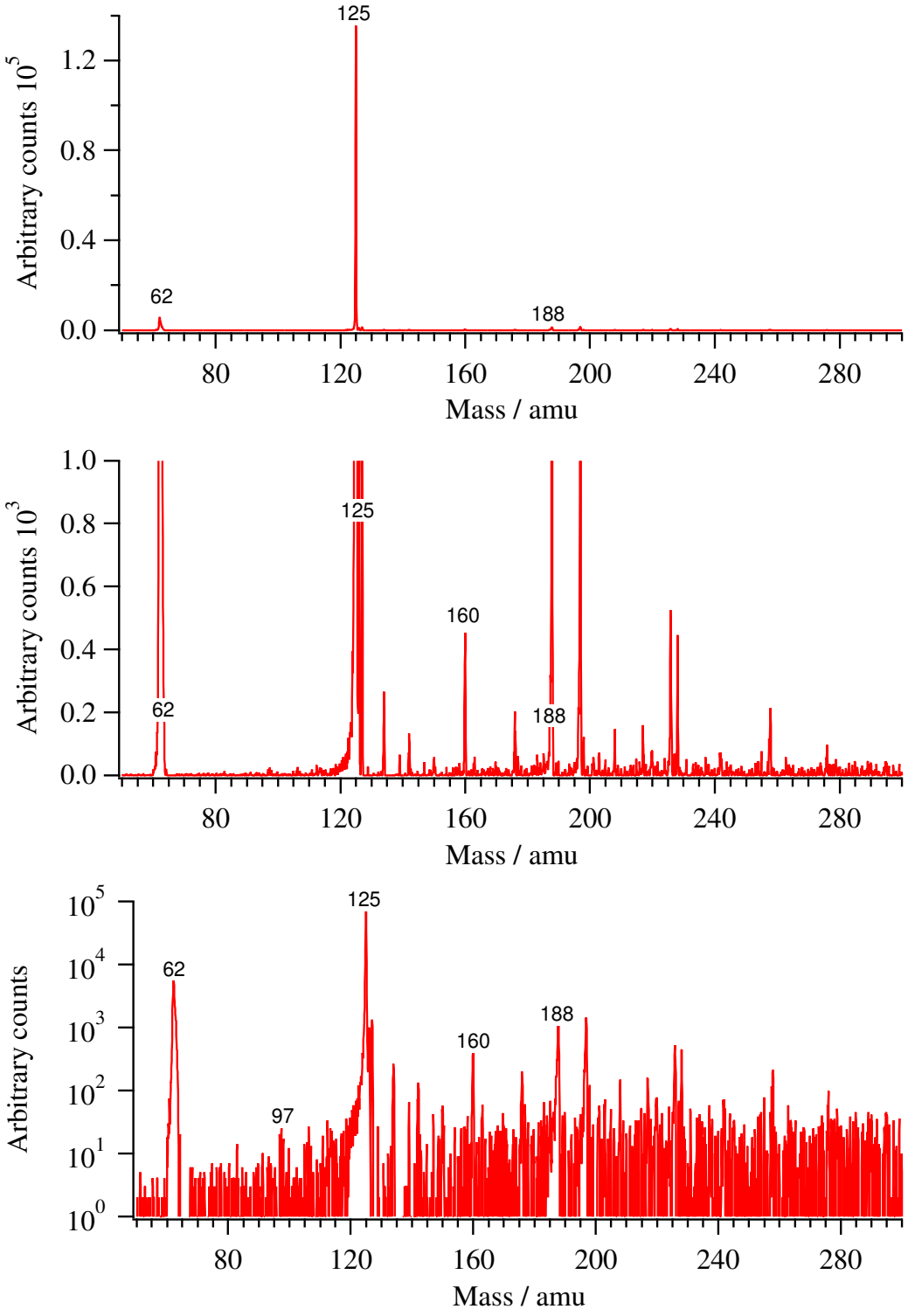

Figure B.1: A typical mass spectrum during normal operation (spectrum no.486 on 16th of March 2004): *First spectrum*: The educt ions 62 (NO_3^-), 125 ($NO_3^-(HNO_3)$) and 188 ($NO_3^-(HNO_3)_2$) are dominant. *Second spectrum*: Same spectrum zoomed; also mass 160 ($HSO_4^-(HNO_3)$) can be seen clearly. *Third spectrum*: Logarithmic y-axis; mass 97 (HSO_4^-).

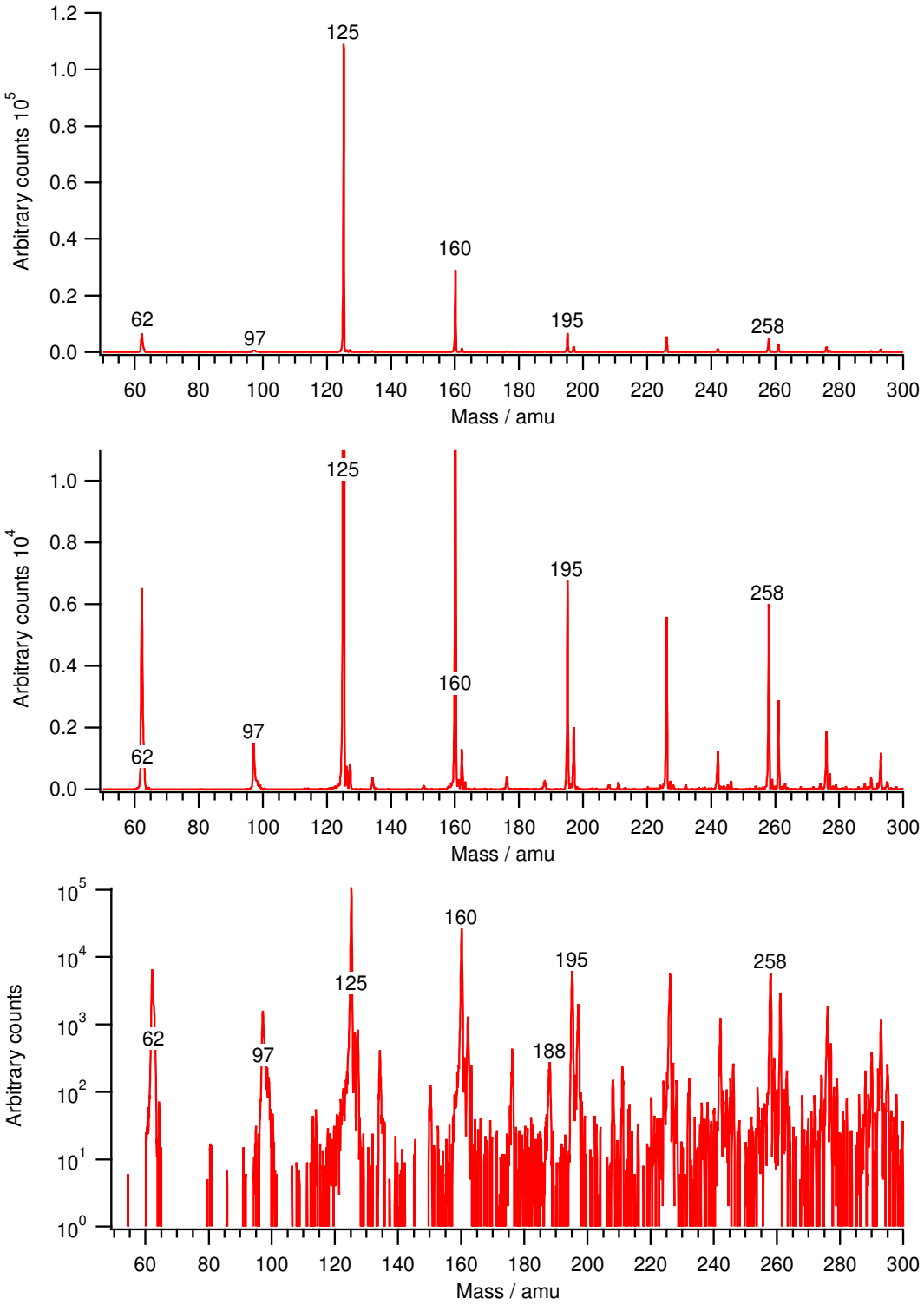

Figure B.2: A typical mass spectrum during calibration (spectrum no.813 on 7th of April 2004): Beside the dominant educt ions also the H_2SO_4 product ions 97 (HSO_4^-), 160 ($HSO_4^-(HNO_3)$) and 195 ($HSO_4^-(H_2SO_4)$) are present.

Appendix C

Experimental Setup

Figure C.1: Photograph of inlet and exhaust (only atmospheric air) system. (The measurement exhaust was filtered via the exhaust system of the MPI.)

Figure C.2: Photograph of complete setup: PITMAS (left), DMPS (middle), exhaust (right).

List of Figures

List of Tables

Bibliography

[Arnold, 1982] Arnold, F. (1982). Ion nucleation - a potential source for stratospheric aerosols. *Nature*, 299:134–137.

[Arnold and Fabian, 1980] Arnold, F. and Fabian, R. (1980). First measurements of gas phase sulfuric acid in the stratosphere. *Nature*, 283:55–57.

[Arnold and Viggiano, 1980] Arnold, F. and Viggiano, A. A. (1980). *Pl. Space Sci.*, 30:1295.

[Arnold, 1978] Arnold, F. und Henschen, G. (1978). First mass analysis of stratospheric negative ions. *Nature*, 275:521–522.

[Aufmhoff, 2004] Aufmhoff, H. (2004). *Atmosphärische gasförmige Vorläufer von Aerosol und Ozon: Messungen mit CIMS-Methoden auf einem Flugzeug und am Boden.* PhD thesis, Universität Heidelberg.

[Boy and Kulmala, 2002] Boy, M. and Kulmala, M. (2002). Nucleation events in the continental boundary layer: Influence of physical and meteorological parameters. *J. of Atmospheric Chemistry and Physics*, 2:1–16.

[Boy et al., 2004] Boy, M., Kulmala, M., Ruuskanen, T., Pihlatie, M., Reissell, A., Aalto, P., Keronen, P., Hellen, H., Hakola, H., Jansson, R., Hanke, M., and Arnold, F. (2004). Sulphuric acid closure and contribution to nucleation mode particle growth. Submitted. *J. of Atmospheric Chemistry and Physics.*

[Boy et al., 2003] Boy, M., Rannik, U., Lehtinen, K., Tarvainen, V., Hakola, H., and Kulmala, M. (2003). Nucleation events in the continental PBL - long term statistical analyses of aerosol relevant characteristics. *J. Geophys. Res.*, 108 (D21):4667.

[Eisele and Tanner, 1993] Eisele, F. and Tanner, D. (1993). Measurements of the gas phase concentrations of H_2SO_4 and methane sulfonic acid and estimates of H_2SO_4 production and loss in the atmosphere. *Journal of Geophysical Research*, 98:9001–9010.

[Finlayson-Pitts and Pitts, 2000] Finlayson-Pitts, B. J. and Pitts, J. N. J. (2000). *Chemistry of the upper and lower atmosphere.* Academic Press, San Diego, London, 1 edition.

[Flood, 1934] Flood, H. (1934). *Z. Phys. Chemie A*, 170:280.

[Fuchs and Sutugin, 1971] Fuchs, N. and Sutugin, A. (1971). Highly dispersed aerosol. *Hidy, G.M. and Brock, J.R. (eds): Topics in current aerosol research, Pergamon, New York.*

[Garrett et al., 2002] Garrett, T., Radke, L., and Hobbs, P. (2002). Aerosol Effects on Cloud Emissivity and Surface Longwave Heating in the Arctic. *Journal of the Atmospheric Sciences*, 59:769–778.

[Hanke, 1999] Hanke, M. (1999). *Development of a Novel Method for Measuring Atmospheric Peroxy Radicals : Calibration, Aircraft-Borne Measurements and Speciated Measurements of HO_2 and RO_2.* PhD thesis, Universität Heidelberg.

[Harshvardhan et al., 2002] Harshvardhan, Schwarz, S., Benkovitz, C., and Guo, G. (2002). Aerosol influence on cloud microphysics examined by satellite measurements and chemical transport modelling. *Journal of the Atmospheric Sciences*, 59:714–725.

[Kim, 2000] Kim, C.S., J. P. (2000). Respiratory dose of inhaled ultrafine particles in healthy adults. *Phil. Trans. R. Soc. Lond. A.*, 358:2693–2705.

[Knop and Arnold, 1985] Knop, G. and Arnold, F. (1985). Nitric acid vapour measurements in the troposphere and lower stratosphere by chemical ionisation mass spectrometry. *Planetary Space Science*, 33/II:983–986.

[Kolb et al., 1994] Kolb, C., Jayne, J., Worsnop, D., Molina, M., Meads, R., and Viggiano, A. (1994). Gas phase reaction of sulphur trioxide with water vapor. *J. Am. Chem. Soc.*, 116:10314–10315.

[Korhonen et al., 1999] Korhonen, P., Kulmala, M., Laaksonen, A., Viisanen, Y., McGraw, R., and Seinfeld, J. (1999). Ternary nucleation of H_2SO_4, NH_3 and H_2O in the atmosphere. *J. Geophys. Res.*, 104:26349–26353.

[Kulmala, 1988] Kulmala, M. (1988). *Nucleation as an aerosol physical problem.* PhD thesis, University of Helsinki.

[Kulmala, 2003] Kulmala, M. (2003). How Particles Nucleate and Grow. *Science*, 302:1000–1001.

[Kulmala et al., 2001] Kulmala, M., Dal Maso, M., Mäkelä, J., Pirjola, L., Väkevä, M., Aalto, P., Miikulainen, P., Hämeri, K., and O'Dowd, C. (2001). On the formation, growth and composition of nucleation mode particles. *Tellus B*, 53:479–490.

[Kulmala et al., 2004a] Kulmala, M., Laakso, L., Lehtinen, K., Riipinen, I., Dal Maso, M., Anttila, T., Kerminen, V., Hõrrak, U., Vana, M., and Tammet, H. (2004a). Initial Steps of Aerosol Growth. *Atmos. Phys. Discuss.*, 4:5433–5454.

[Kulmala et al., 2004b] Kulmala, M., Vehkamäki, H., Petäjä, T., Dal Maso, M., Lauri, A., Kerminen, V.-M., Birmili, W., and McMurry, P. (2004b). Formation and growth rates of ultrafine atmospheric particles: A review of observations. *J. Aerosol Science*, 35-2:143–176.

[Laakso et al., 2003] Laakso, L., Grönholm, T., Rannik, U., Kosmale, M., Fiedler, V., Vehkamäki, H., and Kulmala, M. (2003). Ultrafine particle scavenging coefficients calculated from 6 years field measurements. *Atmospheric Environment*, 37:3605–3613.

[Lovejoy et al., 1996] Lovejoy, E., Hanson, D., and Huey, L. (1996). Kinetics and products of the gas phase reaction of so_2 with water. *J. Phys. Chem.*, 100:19911–19916.

[Mäkelä et al., 2000] Mäkelä, J., Dal Maso, M., Laaksonen, A., Kulmala, M., Pirjola, L., Keronen, P., and Laakso, L. (2000). Characteristics of the aerosol particle formation events observed at a boreal forest site in southern Finland. *Boreal Environment Research*, 5:299–313.

[March and Hughes, 1989] March, R. and Hughes, R. (1989). *Quadrupole Storage Mass Spectrometry*. John Wiley & Sons, New York.

[Mathieu, 1868] Mathieu, E. (1868). Memoire sur le mouvement vibratoire d´une membrane de forme elliptique. *J. Math. Pures Appl.*, 13:137.

[McLachlan, 1947] McLachlan, N. (1947). *Theory and Applications of Mathieu Functions*. Clarendon, Oxford.

[Menon and Saxena, 1998] Menon, S. and Saxena, V. (1998). Role of sulfates in regional cloud-climate interactions. *Atmos. Research*, 47-48:299–315.

[Neumann and Döring, 1940] Neumann, K. and Döring, W. (1940). *Z. Phys. Chemie A*, 186:203.

[Paul and Raether, 1955] Paul, W. and Raether, M. (1955). Das elektrische Massenfilter. *Zeitschrift für Physik*, 140:161–273.

[Paul et al., 1958] Paul, W., Reinhard, H., and von Zahn, U. (1958). Das elektrische Massenfilter als Massenspektrometer und Isotopentrenner. *Zeitschrift für Physik*, 152:143–182.

[Paul and Steinwedel, 1953] Paul, W. and Steinwedel, H. (1953). Ein neues Massenspektrometer ohne Magnetfeld. *Zeitschrift für Naturforschung*, pages 448–450.

[Ramanathan et al., 2001] Ramanathan, V., Crutzen, P., Kiehl, J., and Rosenfeld, D. (2001). Aerosol, climate, and the hydrological cycle. *Science*, 294:2119–2124.

[Reimann, 2000] Reimann, J. (2000). Entwicklung und Aufbau einer Kalibrationsquelle für OH-, HO_2- und RO_2-Radikale. Diplomarbeit, Universität Heidelberg.

[Reiner and Arnold, 1993] Reiner, T. and Arnold, F. (1993). Laboratory flow reactor measurements of the reaction $SO_3 + H_2O + M \rightarrow H_2SO_4 + M$: Implications for gaseous H_2SO_4 and aerosol formation in the plume of jet aircraft. *Geophysical Research Letters*, 20:2659–2662.

[Reiner and Arnold, 1994] Reiner, T. and Arnold, F. (1994). Laboratory investigations of gaseous sulfuric acid formation via $SO_3 + H_2O + M \rightarrow H_2SO_4 + M$: Measurements of the rate constant and products identification. *J. Chem. Phys.*, 101:7399–7407.

[Reiss, 1950] Reiss, H. (1950). *J. Chem. Phys.*, 18:840.

[Scholz, 2004] Scholz, S. (2004). Messung der atmosphärischen Spurengase Schwefelsäure und Methansulfonsäure mittels Ionen-Molekül-Reaktions-Massenspektrometrie. Diplomarbeit, Universität Heidelberg.

[Seinfeld and Pandis, 1998] Seinfeld, J. and Pandis, S. N. (1998). *Atmospheric Chemistry and Physics*. John Wiley & Sons, Inc.

[Stauffer, 1976] Stauffer, D. (1976). *Journal of Aerosol Science*, 7:319.

[Stieb et al., 2002] Stieb, D. M., Judek, S., and Burnett, R. T. (2002). Meta-analysis of time-series studies of air pollution and mortality: Effects of gases and particles and their influence of cause of death, age and season. *J. Air and Manage. Assoc.*, 52:470–484.

[Uecker, 2002] Uecker, J. (2002). *Messung der atmosphärischen Radikale OH, HO_2, RO_2 sowie des Ultraspurengases H_2SO_4 - Weiterentwicklung, Kalibration und Einsatz einer hochempfindlichen massenspektrometrischen Analysemethode.* PhD thesis, Universität Heidelberg.

[Viggiano et al., 1997] Viggiano, A., Seeley, J., Mundis, P., Williamson, J., and Morrison, R. (1997). Rate constants for the reaction of $XHO_3^-(H_2O)$(X=C, HC and N) and $NO_3^-(HNO_3)_n$ with H_2SO_4: Implications for atmospheric detection of H_2SO_4. *Journal of Physical Chemistry A*, 101:8275–8278.

[Volmer, 1939] Volmer, M. (1939). Kinetik der Phasenbildung. *Verlag Von Theodor Steinkopff, Dresden und Leipzig.*

[Wayne, 2000] Wayne, R. P. (2000). *Chemistry of Atmospheres.* Oxford University Press.

[Weber et al., 1997] Weber, R., Marti, J., McMurry, P., Eisele, F., Tanner, D., and Jefferson, A. (1997). Measurements of new particle formation and ultrafine particle growth at a clear continental site. *Journal of Geophysical Research*, 102:4375–4385.

[Wichmann and Peters, 2000] Wichmann, H.-H. and Peters, A. (2000). Epidemiological evidence of the effects of ultrafine particle exposure. *Phil. Trans. R. Soc. Lond. A.*, 358:2751–2769.

[Wollny, 1998] Wollny, A. (1998). Flugzeugmessungen atmosphärischer Spurengase mittels Ionen-Molekül-Reaktions-Massenspektrometrie: Methodische Untersuchungen zur Reaktionskinetik. Master's thesis, Universität Heidelberg.

[Yue and Chan, 1979] Yue, G. and Chan, L. (1979). Theory of formation of aerosols of volatile binary solutions through the ion-induced nucleation process. *J. Colloid Interface Sci.*, 68:501.